

ON ORIGIN AND DESTRUCTION OF RELATIVISTIC DUST AND ITS IMPLICATION FOR ULTRAHIGH ENERGY COSMIC RAYS

THIEM HOANG^{1,2}, A LAZARIAN³, AND R SCHLICKEISER²

Draft version January 17, 2019

ABSTRACT

Dust grains may be accelerated to relativistic speeds by radiation pressure of luminous sources, diffusive shocks, and other acceleration mechanisms. Such relativistic grains have been suggested as potential primary particles of ultrahigh energy cosmic rays (UHECRs). In this paper, we reexamine this idea by studying in detail different destruction mechanisms for relativistic grains moving with Lorentz factor γ through a variety of environment conditions. For the solar radiation field, we find that *sublimation/melting* is a dominant destruction mechanism for silicate grains and large graphite grains. Using an improved treatment of photoelectric emission, we calculate the closest distance that relativistic grains can approach the Sun before destroyed by *Coulomb explosions*. A range of survival parameters for relativistic grains (size a and γ) against both sublimation and Coulomb explosions by the solar radiation field is identified. We also study collisional destruction mechanisms, consisting of *electronic sputtering* by ions and *grain-grain collisions*. Electronic sputtering by light ions is found to be rather inefficient, whereas the evaporation induced by grain-grain collisions is shown to be an important mechanism for which the $a \leq 1 \mu\text{m}$ grains can be completely destroyed after sweeping a column of gas and dust $N_{\text{coll}} \leq 4 \times 10^{20} \text{cm}^{-2}$. The destruction of relativistic dust by the interstellar radiation field (ISRF) and cosmic microwave background (CMB) in the intergalactic medium by melting is inefficient, while Coulomb explosions are only important for grains of very large γ . The obtained results indicate that relativistic dust grains from extragalactic sources would likely be destroyed in the interstellar medium, but the grains accelerated to relativistic speeds in our Galaxy are not completely ruled out as primary particles of UHECRs.

Subject headings: Cosmic rays, ISM: dust-extinction, kinematics and dynamics

1. INTRODUCTION

During the last several years, we have witnessed significant progress in the understanding of ultrahigh energy ($E > 10^{20} \text{eV}$) cosmic rays (UHECRs) thanks to large collaborative research, including Pierre Auger Observatory (Abraham et al. 2007), HiRes (Abbasi et al. 2008), and Telescope Array (Sokolsky 2013). However, the nature of primary particles of UHECRs remains unclear (see Berezhinsky et al. 2006 for a review). The idea of primary protons for UHECRs is challenged by the fact that highest energy protons, presumably coming from extragalactic sources, are likely destroyed via pion photoproduction due to their interactions with CMB photons, such that the cutoff of cosmic ray (CR) spectrum, namely GZK cutoff (Greisen 1966; Zatsepin & Kuz'min 1966), occurs at $\sim 6 \times 10^{19} \text{eV}$. This idea also contradicts with available measurements of CR compositions, which show a significant fraction of heavy nuclei.

Spitzer (1949) has noticed that dust grains could be accelerated to speeds close to that of light by radiation pressure from supernovae. These relativistic grains are thought to gradually disintegrate into heavy nuclei (e.g., Mg, O, Si, Fe, C) due to collisions with gaseous atoms in the interstellar medium (ISM; see also Alfvén 1954).

Later on, motivated by the detection of an extensive air shower which might require primary particles of energy $E > 10^{20} \text{eV}$ (Suga et al. 1971), Hayakawa (1972a) suggested that relativistic dust grains could be a potential candidate for UHECRs above 10^{20}eV . Relativistic dust was once referred to explain cosmic gamma-ray bursts (Grindlay & Fazio 1974).

The Hayakawa's idea seems straightforward. Indeed, a relativistic, spherical grain of size a moving with velocity $v = \beta c$ and Lorentz factor $\gamma = (1 - \beta^2)^{-1/2} \gg 1$ has kinetic energy $E_{\text{gr}}(a, \gamma) = (\gamma - 1)m_{\text{gr}}c^2 \approx 7.06 \times 10^{19}(\gamma/10)\hat{\rho}a_{-5}^3 \text{eV}$, where $a_{-5} = a/10^{-5} \text{cm}$, $\hat{\rho} = \rho/3 \text{g cm}^{-3}$ with ρ mass density within the grain, and $m_{\text{gr}} = (4\pi/3)\rho a^3 = 10^{-14}\hat{\rho}a_{-5}^3 \text{g}$ is the grain mass. Therefore, the relativistic grain of $a = 0.1 \mu\text{m}$ and $\gamma \sim 10$ carries energy $E \sim 10^{20} \text{eV}$, which is sufficient to account for superGZK particles.

Yet the hypothesis of relativistic dust as primary particles of UHECRs has not been well received, possibly, due to the following problems. First, relativistic grains might be destroyed in the solar radiation field before reaching the Earth atmosphere by a process so-called Coulomb explosion (Herlofson 1956). The Coulomb explosion occurs when the tensile strength caused by grain positive charge exceeds the maximum limit that the grain material can support. Berezhinskii & Prilutskii (1977) found that relativistic grains with $\gamma > 25$ would be disrupted by Coulomb explosions. Elenskii & Suvorov (1977) proposed a survival mechanism for relativistic grains based on ion field emission from the grain surface and found that grains between $a \sim 0.03 - 0.06 \mu\text{m}$

¹ Canadian Institute for Theoretical Astrophysics, University of Toronto, 60 St. George Street, Toronto, ON M5S 3H8, Canada; hoang@cita.utoronto.ca

² Institut für Theoretische Physik, Lehrstuhl IV: Weltraum- und Astrophysik, Ruhr-Universität Bochum, D-44780 Bochum, Germany

³ Department of Astronomy, University of Wisconsin-Madison, Madison, WI 53705, USA

and $\gamma < 360$ could reach the Earth without Coulomb explosions. However, both Berezhinsky & Prilutsky (1973) and Berezhinskii & Prilutskii (1977) considered Coulomb explosions assuming a constant photoelectric yield $Y_{pe} = 0.1$, which did not take into account the emission of Auger and secondary electrons, and the dependence of yield on grain charge. This paper is aimed to calculate the exact photoelectric yield as functions of grain size, charge, and the Lorentz factor γ .

Second, relativistic grains may melt when heated above their melting point by the solar radiation field. McBreen et al. (1993) have investigated the interaction of relativistic grains with the solar radiation field, and found that iron grains are likely to melt but carbonaceous grains can survive. They also suggested that the iron grains with $E < 10^{19}$ eV if coming from the direction opposite to the Sun would survive the melting. This study adopted a constant, high emission efficiency (~ 0.5) for all grain sizes, which is much higher than the exact value given by the Planck-averaged emission efficiency. As a result, the grain equilibrium temperature is largely underestimated. Moreover, detailed studies show that, for high-energy photons, only a fraction of the photon energy is transferred into grain vibrational energy while the rest is carried away by photoelectrons (Dwek & Smith 1996). The present paper takes these effects into accounts.

Bingham et al. (1999) revisited the problem of grain charging by photoelectric emission using inverse Compton scattering theory and derived a critical value $\gamma_{cr} \sim 10^4$ below which relativistic grains would not be destroyed by Coulomb explosions. This critical value appears to be much higher than earlier estimates by Berezhinskii & Prilutskii (1977) and Elenskii & Suvorov (1977). It is noted that the Compton treatment in Bingham et al. (1999), which treats all electrons of atoms in the dust grain as free electrons, is only valid for $\gamma h\nu$ much larger than the bonding energy of atomic electrons. For K-shell electrons of iron grains with $E \sim 7000$ eV, this requires $h\nu > 10^4$ eV, or $\gamma \geq 10^4$ with solar photons. Thus, an improved treatment of grain charging for $\gamma < 10^4$ is needed before any reliable conclusion on the survival of these grains can be made.

While radiative destruction by solar photons has been studied by a number of aforementioned authors, collisional destruction by collisions of ions (neutrals) from ambient plasma with relativistic grains is not yet studied in detail. In the frame of reference fixed to the relativistic grain, ions have energy $E > 1$ GeV for $\gamma \gg 1$. Such energetic ions can pass swiftly through the interstellar grains (size likely $a \leq 1 \mu\text{m}$) while transferring part of their energy to dust atoms. Most of the energy loss of ions in the grain is expended to produce electronic excitations and ionizations (Fano 1963; Inokuti 1971). Heavy ions can produce a large number of ionizations along the ion path, for which the Coulomb repulsive force between nearby ions can produce a damage track in the grain (Fleischer et al. 1965; Itoh et al. 2009) and heat diffusion of secondary electrons can impulsively produce a hot cylinder. As a result, some atoms from the hot ionization track near surface can be ejected from the grain surface (sputtering) (see e.g., Bringa & Johnson 2004), which is important for grain destruction.

The destruction of relativistic grains by sputtering in

the Galaxy was briefly discussed in Dasgupta (1979). The study extrapolated the sputtering yield theoretically obtained from the knock-on sputtering regime (the low-energy regime $E < 1$ MeV) for the $E > 1$ GeV range. They obtained a rather low sputtering yield ($Y_{sp} \sim 10^{-6}$) and concluded that sputtering is inefficient for the destruction of relativistic grains. However, modern understanding on sputtering indicates that, in the high-energy regime ($E > 1$ MeV), the electronic sputtering induced by electronic excitations is important (see Johnson & Schou 1993 for a review). Thus, we will use the electronic sputtering model to calculate sputtering yields and resulting destruction rate for relativistic grains.

When a relativistic grain comes into the Earth's atmosphere, it will produce a huge EAS corresponding to the superposition of $N_n \sim m_{gr}/m_H \approx 6.0 \times 10^9 \hat{\rho} a_{-5}^3$ shower events initiated by protons of mass m_H . This is because the mutual interaction between atoms within the grain is negligible compared to their kinetic energy, such that the grain's atoms can interact independently with atomic nuclei in the atmosphere. Observational measurements for the depth of maximum EASs suggest that the relativistic grains of size $a > 0.01 \mu\text{m}$ could not reproduce air showers as observed (Linsley 1980). This result does not support theoretical predictions in Elenskii & Suvorov (1977) that the $a \sim 0.03 - 0.06 \mu\text{m}$ grains with $\gamma < 360$ would be able to reach the Earth atmosphere and produce EASs. Moreover, the measurements from Linsley (1980) seemed to be in favor of EASs produced by primary protons and electrons.⁴ Recently, detailed simulations of EASs triggered by dust grains in Anchordoqui (2000) suggest that the hypothesis of relativistic dust on EASs cannot be ruled out completely.

Observational results from Auger array reveal that active galactic nuclei (AGNs), which are believed to be able to accelerate protons and nuclei to $E \sim 10^{21}$ eV, would be a potential source of UHECRs. The predicted spectra based on AGNs are also in a good agreement with observational data (see Berezhinsky et al. 2006). Earlier Auger data (Abraham et al. 2007) show a strong correlation of the direction of highest CR events with the position of AGNs, but Abbasi et al. (2008) found no such a correlation in the northern hemisphere. Latest results (Abreu et al. 2010) reduce the fraction of the correlation of highest energy events with AGN sources from 69 to 38%, with a fraction of 25% for isotropy. It encourages us to reconsider the problem of relativistic dust using latest understanding on grain destruction processes and realistic models of dust grains.

Our improvements for the relativistic dust idea in this paper include the followings. First, we study in detail the interactions of photons and ions with relativistic grains moving with arbitrary γ , taking into account effects of incident photons, secondary and Auger electrons. For radiative destruction, we compute equilibrium temperatures for grains heated by the full spectrum of the radiation fields and take into account collisional heating by energetic ions passing through the grain. For Coulomb explosions, we calculate grain charges using improved photoelectric emission models. Second, we investigate

⁴ They found that the depth of maximum showers is deep into the atmosphere whereas the air shower by the $a > 0.01 \mu\text{m}$ relativistic grains is expected to have a low depth of ~ 100 km.

the new *collisional destruction* mechanisms due to electronic sputtering and grain-grain collisions, which are disregarded in earlier works. Third, we consider the destruction processes of relativistic grains moving in different astrophysical environments, including solar system, interstellar medium, and intergalactic medium. Our principal goal of this detailed study is to address a long-standing question: whether relativistic grains could survive in the intergalactic medium (IGM), ISM, as well as solar system, and reach the Earth atmosphere as primary particles of UHECRs.

The structure of the paper is as follows. In Section 2 we discuss the potential acceleration mechanisms that can accelerate grains to relativistic speeds. In Section 3 we summarize the transformations of radiation energy and photon density from a stationary to a comoving frame fixed to the dust grain, and briefly discuss the interaction between photons and relativistic grains. Various interaction processes between relativistic grains and ions, electrons, and neutrals in plasma are discussed in Section 4. Grain heating by the solar radiation field and grain destruction by melting/sublimation is studied in Section 5. Photoelectric emission and grain destruction by Coulomb explosions are studied in 6. The destruction of relativistic grains by electronic sputtering and grain-grain collisions is studied in Section 7. An extended discussion and summary are presented in Section 8 and 9.

2. ASTROPHYSICAL SOURCES OF RELATIVISTIC DUST

2.1. Acceleration by radiation pressure

2.1.1. Grain survival near luminous radiation source

Assuming that a radiation source of bolometric luminosity L suddenly ignites, dust grains in the surrounding medium are rapidly heated. Since the radiation flux decreases with increasing distance r from the source as L/r^2 , grains close to the source can be heated above the sublimation temperature and then be destroyed. The closest distance that dust can survive the sublimation is equal to

$$r_{\text{sub}} = \left(\frac{L_{\text{UV}}}{5 \times 10^{12} L_{\odot}} \right)^{1/2} \left(\frac{T_{\text{sub}}}{1800 \text{ K}} \right)^{-5.6/2} \text{ pc}, \quad (1)$$

where L_{UV} is the luminosity in the optical and UV, which is roughly one half of the bolometric luminosity, L_{\odot} is the solar luminosity, T_{sub} is the dust sublimation temperature, and the radiation attenuation is disregarded (see Scoville & Norman 1995; also Appendix A).

Quasars and Seyfert galaxies are strong emitters of X-rays, which are expected to be important for grain destruction via Coulomb explosions due to the accumulation of large positive charge. However, it was estimated in Scoville & Norman (1995) that only small $< 0.01 \mu\text{m}$ grains are destroyed while larger grains would survive at $r \sim 1 \text{ pc}$.

2.1.2. Maximum Velocities

The radiation pressure force acting on a grain of size a at distance r from the radiation source is given by

$$F_{\text{rad}} = \frac{L}{4\pi r^2 c} \langle Q_{\text{pr}}(a, \lambda) \rangle \pi a^2, \quad (2)$$

where $Q_{\text{pr}}(a, \lambda) \pi a^2$ is the radiation pressure cross-section, and the angle brackets $\langle \dots \rangle$ denotes the average

over the radiation spectrum (see Draine 2011). The decrease of radiation intensity by dust extinction, which is small for dust near the sublimation zone, has been disregarded.

Disregarding the minor contribution of gravitational force on the grain, the rate of velocity increase over time for a *non-relativistic grain* is given by the usual equation:

$$\frac{dv}{dt} = \frac{F_{\text{rad}}}{m_{\text{gr}}}, \quad (3)$$

which becomes

$$v dv = \frac{L}{4\pi c m_{\text{gr}}} \langle Q_{\text{pr}}(a, \lambda) \rangle \pi a^2 \frac{dr}{r^2}, \quad (4)$$

where F_{rad} from Equation (2) and $dt = dr/v$ have been used.

Integrating the above equation from the initial distance r_i to r , we obtain

$$v^2 = \frac{L}{2\pi c m_{\text{gr}}} \langle Q_{\text{pr}}(a, \lambda) \rangle \pi a^2 \left(\frac{1}{r_i} - \frac{1}{r} \right), \quad (5)$$

where the grain initially is assumed to be at rest. Equation (5) shows that the grain velocity at $r \gg r_i$ is mainly determined by its initial distance r_i .

Supernovae (type Ia and type II) have luminosity $L \sim 10^8 L_{\odot}$. Thus, silicate grains with sublimation temperature $T_{\text{sub}} = 1800 \text{ K}$ may survive beyond $r_{\text{sub}} \sim 10^{16} \text{ cm}$. Plugging $r_i = r_{\text{sub}}$ and L into Equation (5), we obtain:

$$v \sim 0.1c \left(\frac{L}{10^8 L_{\odot}} \right)^{1/2} \left(\frac{\langle Q_{\text{pr}} \rangle}{1.5} \right)^{1/2} \left(\frac{r_i}{10^{16} \text{ cm}} \right)^{-1/2} a_{-5}^{-1/2}. \quad (6)$$

Quasars or Seyfert galaxies have typical luminosity $L \sim 10^{13} L_{\odot}$, which yields $r_{\text{sub}} \sim 1 \text{ pc}$ for silicate grains. Equation (6) reveals that dust grains can achieve speeds $v = 1.1c$! Such unphysical speeds are a direct result of using Equation (6) that is derived for the *non-relativistic* case.

When the grain is being accelerated to a *relativistic speed*, the equation of motion for the radial component of grain velocity is derived in Robertson (1937) as follows:

$$m_{\text{gr}} c \frac{d\tilde{u}}{ds} = \frac{L}{4\pi r^2 c} \langle Q_{\text{pr}} \rangle \pi a^2 w (1 - w\tilde{u}), \quad (7)$$

where ds is the proper time, $\tilde{u} = (\gamma^2 - 1)^{1/2}$ and $w = \tilde{u} - \gamma$. With $dr = c\tilde{u}ds$, the above equation can be rewritten as

$$m_{\text{gr}} c \tilde{u} d\tilde{u} = \frac{L}{4\pi r^2 c} \langle Q_{\text{pr}} \rangle \pi a^2 (\tilde{u} - \gamma) (1 + \gamma\tilde{u} - \tilde{u}^2) \frac{dr}{c\tilde{u}}, \quad (8)$$

or

$$\frac{\tilde{u} d\tilde{u}}{(\tilde{u} - \gamma)(1 + \gamma\tilde{u} - \tilde{u}^2)} = \frac{L}{4\pi m_{\text{gr}} c^3} \langle Q_{\text{pr}} \rangle \pi a^2 \frac{dr}{r^2}. \quad (9)$$

Integrating the above equation from $r = r_i$ to $r = r_f \gg r_i$ with $u_i = 0$ yields

$$\frac{3L \langle Q_{\text{pr}} \rangle}{16\pi c^3 \rho a r_i} = \frac{1}{3\sqrt{2}} \left[(A+1)^{3/2} + (A-1)^{3/2} - 3(A+1)^{1/2} \right] + \frac{1}{3}, \quad (10)$$

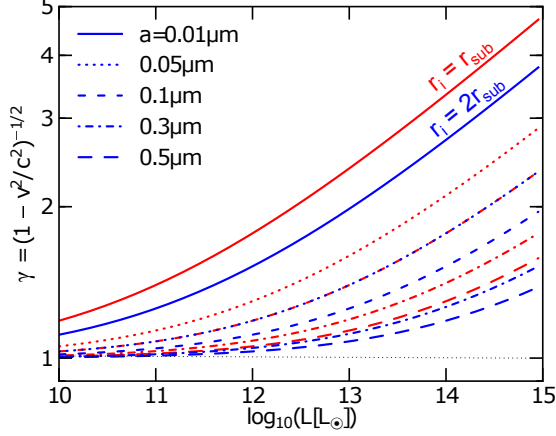


FIG. 1.— Lorentz factor $\gamma = (1 - v^2/c^2)^{-1/2}$ of grains accelerated by radiation pressure as a function of the luminosity of the radiation source for different grain sizes. Grains initially are at rest at distance $r_i = r_{\text{sub}}$ (red lines) and $r_i = 2r_{\text{sub}}$ (blue lines). Silicate grains and $\langle Q_{\text{pr}} \rangle = 1.5$ are considered.

where $A = 1 + 2\tilde{u}^2 = 2\gamma^2 - 1$ (Noerdlinger 1971). Plugging in the numerical parameters, we obtain

$$l.h.s = 1.3 \times 10^7 \left(\frac{L}{10^{13} L_{\odot}} \right) \left(\frac{\langle Q_{\text{pr}} \rangle}{1.5} \right) \left(\frac{r_i}{1 \text{ pc}} \right) a_{-5}^{-1}. \quad (11)$$

For a given L , solving Equation (10) gives us the terminal A and the Lorentz factor γ that the grain is accelerated to. Figure 1 shows the achieved γ as a function of L for different grain sizes for $r_i = r_{\text{sub}}$ and $r_i = 2r_{\text{sub}}$. It can be seen that, for bright quasars or Seyfert galaxies, radiation pressure can accelerate dust grains to relativistic speeds with $\gamma < 5$.

2.1.3. Effects of Gas Drag

Maximum grains velocities accelerated by radiation pressure (e.g., Eq. 5) were obtained by disregarding the drag force arising from ambient gas. To see its importance on grain deceleration, let us estimate the acceleration time by radiation pressure and compare it with the drag time.

The acceleration time by radiation pressure is given by

$$\tau_{\text{acc}} = \frac{v}{|dv/dt|} = \frac{m_{\text{gr}} v}{F_{\text{rad}}} = \frac{m_{\text{gr}} v A \pi r^2 c}{\langle Q_{\text{pr}} \rangle \pi a^2 L}, \quad (12)$$

$$= 1.1 \times 10^6 \hat{\rho} a_{-5} r_{\text{pc}}^2 \frac{1.0}{\langle Q_{\text{pr}} \rangle} \left(\frac{v}{0.01c} \right) \left(\frac{L}{10^{13} L_{\odot}} \right)^{-1} \text{ s}, \quad (13)$$

r_{pc} is the distance of the grain in units of pc. Thus, grains can be accelerated to $v \sim c$ in $\sim 10^8$ s or after moving a distance ~ 1 pc for $L \sim 10^{13} L_{\odot}$.

For v much larger than the thermal velocity of gaseous atoms under our interest, gas drag due to Coulomb collisions by ions is subdominant, and the drag force can be given by (see Draine 2011)

$$F_{\text{drag}} = n_{\text{gas}} \mu_{\text{gas}} m_{\text{H}} v^2 \pi a^2, \quad (14)$$

where n_{gas} is the gas number density, and μ_{gas} is the mean molecular weight of the gas.

Thus, the drag time is equal to:

$$\tau_{\text{drag}} = \frac{m_{\text{gr}} v}{F_{\text{drag}}} = \frac{m_{\text{gr}}}{n_{\text{gas}} \mu_{\text{gas}} m_{\text{H}} v \pi a^2}, \quad (15)$$

$$= 7.9 \times 10^9 \hat{\rho} a_{-5} \mu_{\text{gas}}^{-1} \left(\frac{n_{\text{gas}}}{10 \text{ cm}^{-3}} \right)^{-1} \left(\frac{v}{0.01c} \right)^{-1} \text{ s} \quad (16)$$

which is simply equal to the time needed for the grain to collide with an amount of gas with mass equal to the grain's mass.

For the diffuse interstellar medium ($n_{\text{gas}} \sim 10 \text{ cm}^{-3}$), Equations (13) and (16) reveal that $\tau_{\text{drag}} \gg \tau_{\text{acc}}$, thus gas drag plays little effect during the acceleration stage. When the grain velocity exceeds $v \sim 0.9c$, $\tau_{\text{drag}} < \tau_{\text{acc}}$, and grains may not be accelerated to higher velocities.⁵ In dense regions with $n_{\text{gas}} \sim 10^4 \text{ cm}^{-3}$, gas drag becomes important for velocity above $v \sim 0.03c$, and grains are unlikely accelerated to $v \sim c$ by radiation pressure.

2.2. Acceleration of subrelativistic grains by collisionless shock

The original idea of grain acceleration by diffuse shocks was first suggested by Epstein (1980), who pointed out that charged grains with high mass-to-charge ratio could be efficiently accelerated in the diffusive shock by the first-order Fermi mechanism as ions. An elaborated study in Ellison et al. (1997) shows that charged grains indeed could be accelerated to high speeds by diffusive shocks. They estimated the maximum grain velocity achieved by the shock as follows:

$$\beta_{\text{max}} \simeq 0.024 \eta^{-1/3} \left(\frac{V_{\text{sh}}}{400 \text{ km s}^{-1}} \right)^{2/3} a_{-5}^{-1/3} n_{\text{gas}}^{-1/3} \phi_{10}^{1/3} B_{10}^{1/3} \quad (17)$$

where the typical value $\eta = 1$, $\phi_{10} = \phi/10V$ with ϕ being grain electric potential, $B_{10} = B/10\mu\text{G}$ with B magnetic field strength, and V_{sh} is the shock velocity.

Assuming a high velocity shock of $V_{\text{sh}} = 10^4 \text{ km s}^{-1}$ (typical shock velocity of a young supernova remnant (SNR) at the end of free-expansion phase), Equation (17) shows that the $0.1 \mu\text{m}$ grains can be accelerated to a velocity $\beta_{\text{max}} \approx 0.2$ or $v \approx 0.2c$ by this shock for the typical magnetic field $B = 10\mu\text{G}$. Moreover, observational and numerical studies reveal that the magnetic field in the shock is substantially amplified (Berezhko et al. 2003; Beresnyak et al. 2009; Riquelme & Spitkovsky 2010). Thus, the maximum grain velocity achieved will be considerably enhanced.

Recently, numerical studies in Giacalone et al. (2009) also show that even charged grains that are initially stationary with respect to the upstream plasma can be accelerated to high speeds (about 10 times the shock speed).

3. INTERACTIONS OF RELATIVISTIC DUST WITH RADIATION

3.1. Lorentz Transformations of Radiation Fields

Before going into detailed discussions on interactions of relativistic dust with radiation, it is useful to summarize the Lorentz transformations of radiation from a stationary frame (hereafter SF) to a comoving frame attached to the grain (hereafter GF).

Assuming that a dust grain is moving with $\gamma \gg 1$ in a radiation field. Let $\mu = \cos \theta$ be the cosine angle between

⁵ The issue of whether the classical drag force (Eq. 14) is still valid for relativistic velocities ($v \sim 0.1c$) where impinging ions are not to stick to the grain will be discussed in our future paper.

the direction of grain motion and that of photon propagation. Let $\nu, u(\nu)$ and $n(\nu)$ be the photon frequency, spectral energy density of radiation, and number density of photons in the SF. The transformations of these quantities from the SF to the GF are presented in Appendix B, here we summarize the most important formulas to be used for calculations.

The photon frequency in the GF reads

$$\nu' = \gamma\nu(1 - \beta\mu). \quad (18)$$

For an *isotropic radiation field*, the spectral and total energy density in the GF are respectively given by

$$u'(\nu')d\nu' = u(\nu)d\nu\gamma^2 \left(1 + \frac{\beta^2}{3}\right), \quad (19)$$

$$u'_{\text{rad}} = u_{\text{rad}}\gamma^2 \left(1 + \frac{\beta^2}{3}\right), \quad (20)$$

where $u_{\text{rad}} = \int d\nu u(\nu)$.

Similarly, for a *point source of radiation*, we have the followings

$$u'(\nu')d\nu' = u(\nu)d\nu\gamma^2(1 - \beta\mu_{\text{gr}})^2, \quad (21)$$

$$u'_{\text{rad}} = u_{\text{rad}}\gamma^2(1 - \beta\mu_{\text{gr}})^2, \quad (22)$$

where $\mu_{\text{gr}} = -1$ for the case grains approach the Sun in the radial direction.

Equations (18) and (20) show that the photon frequency (also energy) is increased by a factor γ , and the energy density of radiation is increased by γ^2 times in the GF. The effect is most significant for grains of large γ .

3.2. Interaction of photons with Relativistic Dust: General Consideration

Below, we briefly discuss the interaction of photons having an arbitrary energy with a stationary dust grain, which is equivalent to the interaction of optical solar photons with a grain moving with arbitrary γ . Our discussions will be focused on the effect of photons in grain heating and emission of photoelectrons, which is important for grain destruction.

3.2.1. Low-energy photons

An incident, low-energy photon ($h\nu < 20 \text{ eV}$) is likely absorbed by the dust grain. When the photon energy $h\nu$ is larger than the ionization potential IP of the grain, it will produce a photoelectron by ionizing an atom mostly from the band structure (see e.g., Weingartner & Draine 2001). The kinetic energy of the photoelectron is equal to $h\nu - \text{IP}$. To escape from the grain surface, the photoelectron must travel a distance from the emitting atom to the surface during which it transfers a significant part of energy to the grain. If the photoelectron has sufficient energy, it will escape from the grain surface to infinity and deposits a positive charge to the grain. For $h\nu < \text{IP}$, the photon energy is solely transferred to the dust through electronic excitations, without producing a photoelectron. Thus, whether producing photoelectrons or not, the entire energy of low-energy photons can be deposited to the dust grain.

3.2.2. High-energy photons

For high-energy photons ($h\nu > 20 \text{ eV}$), we can treat their interaction with the dust grain as atomic interaction, i.e., interaction of photons with individual atoms within the grain. After the absorption of an energetic photon, an electron from some *inner shell* is excited and can become a photoelectron.

After the photoelectron is produced from the inner shell of low-energy level i , it also leaves a hole (opening). This hole can be filled by an electronic transition from a higher energy level j . Such an electronic transition can be done through radiativeless (Auger) process accompanied by the ejection of a second electron (namely Auger electron) from some allowed energy level k . The Auger electron due to the (i, j, k) transition also deposits some energy to the grain and becomes a free electron if it has sufficiently strong energy. The second process is through a radiative (fluorescent) transition. Theory indicates that, for X-ray energy, the Auger transition is dominant. After an Auger transition, the atom is doubly ionized, with one hole in j shell and another in k shell. These j and k holes can be filled by radiativeless transitions from j' and k' shells, producing secondary Auger electrons. This process continues until all Auger transitions have been used, and the atom is multiply ionized (see Dwek & Smith 1996).

A different process related to the initial ionization of i -shell is that, following the ionization, the atom is left on the excited state with energy equal to the binding energy E_i . This is called residual excitation energy. Then, the atom de-excites to a lower energy level, releasing a photon. Such a photon is likely being absorbed by the dust. Therefore, the detailed calculation of grain heating by X-ray requires the knowledge on the fraction of photon energy is deposited to the grain and that is carried away by free photoelectrons.

3.2.3. Very high-energy photons

For very high-energy photons $h\nu > 10^4 \text{ eV}$, the dust grain appears transparent to radiation, and we can treat the interaction of photons with the dust grain as the interaction of photons with free electrons. During each scattering, the photon transfers some of its energy to the electron via inverse Compton effect, resulting in the recoil of the electron. The scattered electron will escape from the grain surface if it has sufficient energy to overcome the potential barrier (Bingham et al. 1999).

For photons with energy above 1 MeV ($\geq 2m_e c^2$), the pair production starts to become important. Each nucleus n in the dust grain interacts with an energetic photon γ_{ph} to produce a pair of electron-positron, which is given by $n + \gamma_{\text{ph}} \rightarrow n + e^+ + e^-$. This additional pair production process might help in explaining the observed high positron fraction in primary cosmic rays by the AMS collaboration (Accardo et al. 2014; Aguilar et al. 2014).

The inverse process to pair production, namely annihilation, can happen when an electron e^- of the dust grain collides with a positron from the ambient plasma. The process is followed by the emission of a photon via $e^- + e^+ \rightarrow 2\gamma_{\text{ph}}$.

3.3. Absorption cross-section

We consider a mixed-dust model that consists of silicate and graphite grains. The complex refractive index m and dielectric functions ϵ for these grain populations is taken from [Draine \(2003\)](#) for photon energy from $h\nu = 1 \text{ eV}$ to 10^4 eV . The absorption efficiency for X-ray, $Q_{\text{abs}} = C_{\text{abs}}/\pi a^2$ with C_{abs} being the absorption cross-section, is exactly computed using the Mie theory code of [Wiscombe \(1980\)](#) for spherical grains with wavelength λ and size parameter $x = 2\pi a/\lambda < 2 \times 10^4$. For $x > 2 \times 10^4$, we use the anomalous diffraction theory ([van de Hulst 1957](#)), which have Q_{abs} given by

$$Q_{\text{abs}} = 1 + \frac{\exp[-4x\text{Im}(m)]}{2x\text{Im}(m)} - \frac{\exp[-4x\text{Im}(m)] - 1}{8x^2\text{Im}^2(m)}, \quad (23)$$

where $\text{Im}(m)$ denotes the imaginary part of m .

To compute Q_{abs} for graphite grains, we consider two cases in which the electric field of radiation \mathbf{E} is parallel and perpendicular to the grain optical axis (c -axis) with the corresponding dielectric function ϵ_{\parallel} and ϵ_{\perp} . Using the (1/3) – (2/3) approximation (i.e., 1/3 of graphite grains have $\epsilon = \epsilon_{\parallel}$ and 2/3 of them have $\epsilon = \epsilon_{\perp}$), one can obtain the extinction cross-section $C_{\text{ext}} = (C_{\text{ext}}(\mathbf{E}||c) + 2C_{\text{ext}}(\mathbf{E} \perp c))/3$ for a given grain orientation.

Figure 2 shows Q_{abs} as a function of photon energy computed using the Mie theory for different grain sizes for silicate (left) and graphite (right) grains.

4. INTERACTIONS OF RELATIVISTIC GRAINS WITH AMBIENT GAS

4.1. General Consideration

Interaction processes between an incident ion and atoms within the dust grain (hereafter target atoms) depend on its initial velocity (energy). When its velocity is smaller than the Bohr velocity of atomic electron $v_0 = e^2/\hbar$ (i.e., energy 25keV/u), the *elastic* interaction regime between the ion and target atomic nuclei is crucial. Above the threshold velocity v_0 , electronic interactions take over, and many physical effects, such as electronic excitation and ionization are triggered.

In the ultrahigh energy regime, *nuclear* interactions between the incident ion and an individual nucleon in the target nuclei become important. For instance, the ion-nucleon collision can first produce pions π^{\pm}, π^0 . The rapid decay of a π^0 will generate two gamma-rays photons, i.e., $\pi^0 \rightarrow 2\gamma_{\text{ph}}$, while the decay of a charged pion π^{\pm} generates neutrinos (ν_{μ}) and muons (μ^{\pm}). However, the nuclear interaction cross-section is rather small and its effect on grain destruction is expected to be less important than the effect by electronic excitations.

For reference, we below summarize principal processes and well-known formulas from stopping theory of swift ions and electrons passing through matter. A classical review can be found in [Fano \(1963\)](#).

4.2. Incident Ions

Consider the collision of an incident ion (projectile) of charge $Z_P e$ and kinetic energy E (velocity βc) with an electron of a target atom in the grain. Let $Z_{T,i}$ be the atomic number of target element i . Initially, the atomic nucleus and electron are considered stationary because their energy is much lower than the energy of the projectile.

In the high-energy regime, the energy loss of incident ion is mainly used to ionize atoms. The total energy loss of the incident ion per pathlength in a material, which is usually referred to as *stopping power* of the material, is given by

$$\frac{dE_{\text{ion}}}{dx} = \sum_i n_i S_i, \quad (24)$$

where n_i is the atomic number density of element i , S_i is the electronic stopping cross-section induced by atoms of element i in units of eV cm^2 , and the sum is taken over all elements i present in the grain. The total atomic number density in the grain is thus $n_d = \sum_i n_i$.

The Bethe-Bloch theory yields the following ([Fano 1963](#)):

$$S_i = 4\pi \frac{(Z_P e^2)^2}{m_e c^2 \beta^2} Z_{T,i} \times \left[\frac{1}{2} \ln \frac{2\gamma^2 m_e c^2 \beta^2 T_{\text{max}}}{I_i^2} - \beta^2 - \frac{C}{Z_{T,i}} - \frac{\delta}{2} \right], \quad (25)$$

where T_{max} is the maximum energy transferred from the ion to the electron, and I_i is the mean excitation energy of element i . Here $C/Z_{T,i}$ is the correction term for inner shells, and $\delta/2$ is the correction term for the polarization effect of target atom induced by the ion.

In binary collisions, the maximum exchange energy is equal to

$$T_{\text{max}} = \frac{2\gamma^2 M_P^2 m_e c^2 \beta^2}{m_e^2 + M_P^2 + 2\gamma m_e M_P}, \quad (26)$$

where M_P is the atomic mass of the projectile.

In the case $2\gamma m_e/M_P \ll 1$ (heavy ion or not really high γ), we have $T_{\text{max}} = 2\gamma^2 \beta^2 m_e c^2$. Thus, Equation (25) can be rewritten as

$$S_i = 4\pi \frac{(Z_P e^2)^2 Z_{T,i}}{m_e c^2 \beta^2} \left[\ln \frac{2m_e c^2 \beta^2}{I_i} + \mathcal{L}(\beta) \right], \quad (27)$$

where

$$\mathcal{L}(\beta) = \ln \frac{1}{1 - \beta^2} - \beta^2 - \frac{C}{Z_{T,i}} - \frac{\delta}{2}. \quad (28)$$

The Bethe-Bloch formula (Eq. 25) with its correction terms is of high accuracy for energetic ions with $E > 1 \text{ MeV}$ under our interest in this paper. Moreover, the term $C/Z_{T,i}$ is negligible for the GeV range. The term δ is important, and we calculate it using an analytical fit from [Sternheimer et al. \(1984\)](#).

4.3. Incident Electrons

4.3.1. Electronic Interactions

An incident energetic electron can interact both with target atomic nuclei and electrons via Coulomb forces. The same as ions, electronic excitation by the incident electron can bring the atom to an excited, bound state or ionization. The total energy loss of a relativistic electron of kinetic energy E per pathlength due to the ionization of target atoms is equal to (see e.g., [Longair 2011](#))

$$\frac{dE_{\text{el}}}{dx} = \sum_i n_{e,i} S_{\text{el},i} \quad (29)$$

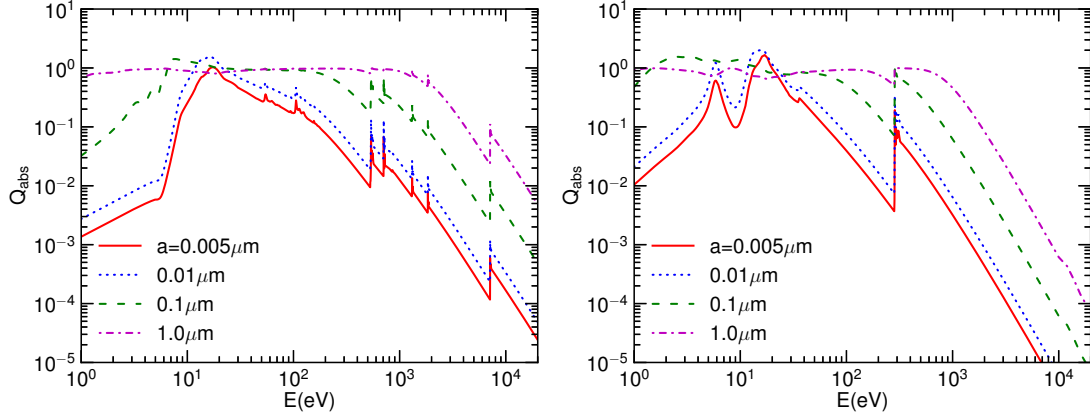


FIG. 2.— Absorption efficiency Q_{abs} as a function of photon energy for different grain sizes for silicate (left) and graphite (right) grains. A sharp spectral feature at $E \approx 291$ eV in the right panel corresponds to the excitation of K-shell of C atom. Several spectral features in silicate grain (left panel) are also due to K-shell excitations of Si, Mg, O and Fe atoms.

where $n_{e,i} = n_i Z_{T,i}$ is the number density of electrons from atom i in the grain,

$$S_{\text{el},i} = \frac{2\pi e^4}{m_e c^2 \beta^2} \left[\ln \frac{\gamma^2 m_e c^2 \beta^2 T_{\text{max}}}{2I_i^2} + \mathcal{F}(\gamma) \right], \quad (30)$$

where

$$\mathcal{F}(\gamma) = -\left(\frac{2}{\gamma} - \frac{1}{\gamma^2}\right) \ln 2 + \frac{1}{\gamma^2} + \frac{1}{8} \left(1 - \frac{1}{\gamma}\right)^2, \quad (31)$$

and T_{max} is the maximum energy of transfer to the target electron.

For electron-electron collisions, Equation (26) yields

$$T_{\text{max}} = \frac{\gamma^2 m_e c^2 \beta^2}{1 + \gamma}. \quad (32)$$

Plugging T_{max} from the above equation to Equation (30), one obtains

$$S_{\text{el},i} = \frac{2\pi e^4}{m_e c^2 \beta^2} \left[\ln \left(\frac{E^2 \gamma + 1}{I_i^2} \right) + \mathcal{F}(\gamma) \right]. \quad (33)$$

4.3.2. Energy loss due to Bremsstrahlung effect

In addition to electronic excitations, while passing the grain, energetic electrons are accelerated in the Coulomb force field of atomic nuclei, and they emit continuous radiation (namely free-free emission) due to the Bremsstrahlung effect.

Bethe & Heitler (1934) derived the total energy loss per pathlength in radiation as the following:

$$\frac{dE_{\text{Brems}}}{dx} = \sum_i n_i \frac{Z_{T,i}^2 r_e^2}{137} E \left[4 \ln \left(\frac{2E}{m_e c^2} \right) - 4/3 \right] \quad (34)$$

for $m_e c^2 < E < 137 m_e c^2 Z_{T,i}^{-1/3}$, and

$$\frac{dE_{\text{Brems}}}{dx} = \sum_i n_i \frac{Z_{T,i}^2 r_e^2}{137} E \left[4 \ln \left(183 Z_{T,i}^{-1/3} \right) + 2/9 \right] \quad (35)$$

for $E > 137 m_e c^2 Z_{T,i}^{-1/3}$. Here $r_e = e^2/m_e c^2$ is the classical electron radius.

The Bremsstrahlung emission spectrum is broad, independent of frequency, ranging from zero frequency up

to $\nu_{\text{max}} = (\gamma - 1)m_e c^2/h = 511 \text{keV}(\gamma - 1)/h$. Low-energy Bremsstrahlung photons are likely absorbed by the grain while high-energy photons can produce higher order photoelectrons. Therefore, some fraction of the photon energy is carried away by scattered photons and photoelectrons. We assume that roughly about 50% of the Bremsstrahlung radiation is absorbed by the grain.

4.4. Incident Neutrals

When an atom is moving at a relativistic speed, its kinetic energy is much larger than the orbital energy of atomic electrons. The incident atom can be considered to be a pair of the ion (nucleus) and electrons that independently interact with target atoms. Atomic excitation and ionization not only occurs with the target atom but also with the projectile atom, which can result in the ionization of the incident atom (see e.g., Sanders et al. 2007). The energy loss of the incident atom is the sum of the energy loss from the ion and electrons:

$$\frac{dE}{dx} = \left(\frac{dE_{\text{ion}}}{dx} \right) + \left(\frac{dE_{\text{el}}}{dx} \right). \quad (36)$$

4.5. Range and mean ionization length in dust grains

The range that a projectile of initial energy E_0 penetrates in solid before completely stopped is defined as the following:

$$R(E_0) = \int_{E_0}^0 \left(\frac{dE}{dx} \right)^{-1} dE, \quad (37)$$

where dE/dx is the stopping power of the projectile.

We calculate the energy loss of incident ions/electrons colliding with relativistic grains of different Lorentz factor γ . To facilitate comparison with available experimental data, we assume the quartz of structure SiO_2 for silicate with mass density $\rho = 3.3 \text{ g cm}^{-3}$, which yields $n_{\text{Si}} = n_{\text{O}}/2 = 3.3 \times 10^{23} \text{ cm}^{-3}$ and $n_d = 10^{23} \text{ cm}^{-3}$.

Figure 3 (left panel) shows the energy loss of a H atom (i.e., a proton and electron) by different processes and its total energy loss. The energy loss of the electron via electronic interaction is dominant until the radiative loss via Bremsstrahlung effect becomes important at $\gamma \sim 100$.

Figure 3 (right panel) shows the total energy loss of selected atoms H, He, C, O, and Fe in a silicate grain. As

expected, heavier ions can have higher energy loss, i.e., can transfer higher amount of energy to the target atoms. The energy loss decreases rapidly with increasing γ up to a minimum at $\gamma \sim 2$ due to the decrease of electronic cross-section. As γ increases, dE/dx rises slowly due to the effect of the transverse component of Coulomb force. For $\gamma > 10^3$, dE/dx rises rapidly due to the radiative loss of electrons via Bremsstrahlung effect.

In solid, the energy loss of swift ions mostly results in ionization of atoms followed by atomic motion (sputtering) and heat transfer. Using the total stopping power dE/dx , we can estimate the mean length between two successive ionizations:

$$\lambda_{\text{ion}} = \frac{W}{dE/dx}, \quad (38)$$

where W is the average energy needed to create an ionization in the grain.

Figure 4 (left panel) shows the range R of different ions as a function of γ for silicate grains. It can be seen that relativistic ions have $R \gg 1 \mu\text{m}$, i.e., they easily pass through the interstellar grains.

Figure 4 (right panel) shows λ_{ion} the mean length between two successive ionization. It can be seen that light ions (i.e., H, He) can create $2a/\lambda_{\text{ion}} \sim 200a_{-5}$ ionization events along their entire path through grain. For the $a < 0.01 \mu\text{m}$ grains, light ions can produce a couple ionizations in their entire trajectory. Fe ions are a significant source of ionizations producing up to ~ 20 ionization events per atomic layer, which forms a track of dense ionizations in the grain referred to as *ionization track*.

5. HEATING OF RELATIVISTIC GRAINS IN THE SOLAR RADIATION FIELD

5.1. Collisional heating

To see the effect of incident ions/atoms on grain heating, it is useful to estimate the average energy transferred to an atom within the grain:

$$\begin{aligned} \Delta E_1 &= l \frac{dE}{dx} \sim n_d^{1/3} \frac{dE}{dx}, \\ &\sim 21.54 n_{23} \left(\frac{dE/dx}{10^9 \text{ eV cm}^{-1}} \right) \text{ eV}, \end{aligned} \quad (39)$$

where l is the mean interatomic distance, $n_{23} = n_d/10^{23} \text{ cm}^{-3}$.

Using dE/dx from Figure 3, we find that a H atom with $dE/dx \sim 3 \times 10^7 \text{ eV cm}^{-1}$ can transfer $\Delta E_1 \sim 21.54 n_{23} \left(\frac{3 \times 10^7}{10^9} \right) \text{ eV} \sim 0.64 n_{23} \text{ eV}$ to a target atom. This energy is not sufficient to create ionizations, and the entire energy loss of H atom is spent to grain heating. He, C and O atoms can provide $\Delta E_1 < 15 \text{ eV}$ to a target atom through photoelectrons.

Fe ions having $dE/dx \sim 6 \times 10^9 \text{ eV cm}^{-1}$ can transfer $\Delta E_1 \sim 130 n_{23} \text{ eV}$ to a target atom. This energy is sufficient to create photoelectrons from the band structure and outer shells, providing secondary electrons with kinetic energy $E_e < 130 \text{ eV}$. The range of these secondary electrons of energy E_e is $R_e \sim 118 \hat{\rho}^{-0.85} (E_e/1 \text{ keV})^{1.5} \text{ \AA}$ (Draine & Salpeter 1979b), which is less than 4 \AA for $E_e \sim 100 \text{ eV}$. Therefore, the secondary electrons produced by impinging Fe

ions quickly lose their energy to the lattice and heat the grain up.

Let f_{coll} be the fraction of the ion energy loss dE/dx that is expended to grain heating. Then, the heating rate due to ion collisions in the GF can be written as

$$\frac{dE_{\text{coll}}}{dt'} = (n_{\text{gas}} \beta c) \pi a^2 \left(f_{\text{coll}} \frac{dE}{dx} \right) \left(\frac{4a}{3} \right), \quad (40)$$

where the grain is approximated as a slab of thickness $4a/3$.

Taking the typical numeric values for dE_{coll}/dt , we can obtain

$$\frac{dE_{\text{coll}}}{dt'} \approx 2 \times 10^{-7} \left(\frac{n_{\text{gas}}}{1 \text{ cm}^{-3}} \right) \beta a_{-5}^3 \left(\frac{f_{\text{coll}}}{1.0} \right) \left(\frac{dE/dx}{10^9 \text{ eV cm}^{-1}} \right) \text{ erg s}^{-1}.$$

As discussed above, it is adequate to adopt $f_{\text{coll}} \sim 1$ for all ions lighter than Fe , and $f_{\text{coll}} \sim 0.5$ for the latter (about half of Fe energy loss goes into ionization). The collisional heating is expected to be important for the ISM but subdominant for the solar radiation field.

5.2. Radiative Heating

Earlier studies on radiative heating of relativistic grains (Hayakawa 1972b; McBreen et al. 1993) assumed that the entire photon energy is converted to grain heating. However, a detailed study on radiative heating by X-ray photons in Dwek & Smith (1996) shows that a considerable fraction of photon energy is carried away by photoelectrons.

Let $f_{\text{dep}}(a, E) = E_{\text{dep}}(a, E)/E$ be the fraction of photon energy deposited to the grain after absorption, where $E_{\text{dep}}(a, E)$ is the energy deposited to the grain after the absorption of a photon of energy $E = h\nu$. Detailed calculations for E_{dep} and f_{dep} are carried out in Dwek & Smith (1996). For our calculations, we adopt their results given in $Q_{\text{abs}} E_{\text{dep}}$ from Table 5.1 and 5.2 in Dwek & Smith (1996) for neutral grains. Below we provide a short summary on major relevant results useful for further discussions.

In the solar radiation field with the averaged photon energy $E \equiv h\bar{\nu} = 1.34 \text{ eV}$, due to the Doppler effect, the optical solar radiation appears as X-ray, with energy $h\bar{\nu}' = \gamma h\bar{\nu}$ up to 10^4 eV for $\gamma = 10^4$ in the grain's reference frame. Such high photon energy is sufficient to excite electrons in the innermost K-shell of atoms followed by numerous physical processes, including Auger transitions and secondary transitions.

The total dependence of f_{dep} on energy is an overall effect, which is determined by the energy-dependence of the energy deposited to the grain by photoelectrons and Auger electrons. For small grains, the energy dependence of f_{dep} is mainly determined by Auger electrons, but for large grains it is dominated by photoelectrons because these photoelectrons lost most of their energy while moving within the grain.

Figure 5 shows the total energy-dependence f_{dep} for silicate (left panel) and graphite (right panel) grains reproduced from Dwek & Smith (1996). It can be seen that the entire photon energy is deposited to the grain for $E < 100 \text{ eV}$, regardless of grain size. Moreover, it shows that f_{dep} starts to decline when the photon energy exceeds some value. The E value at which f_{dep} starts to fall rapidly tends to be smaller for smaller grains. Thus,

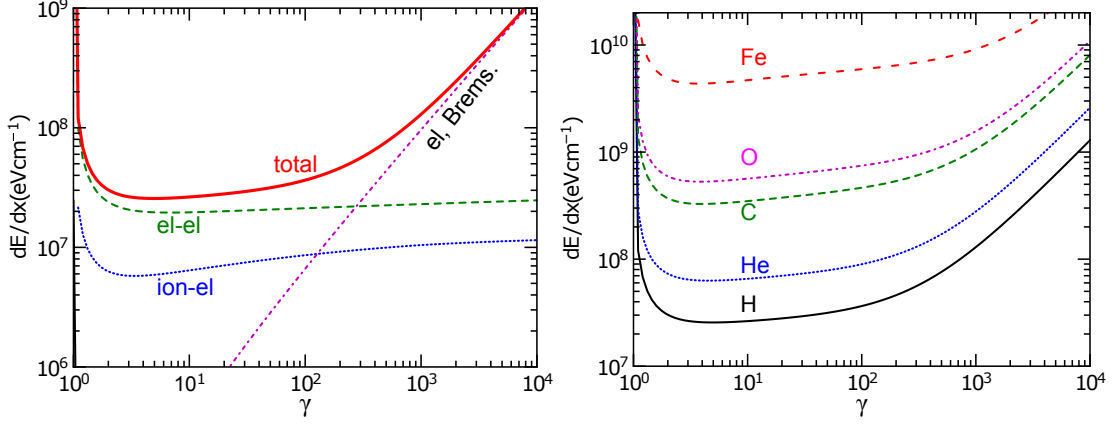


FIG. 3.— Left panel: energy loss per pathlength (eV cm^{-1}) of a H atom in silicate material as a function of the Lorentz factor γ . Individual interaction processes between the ion/electron with the target nucleus/electron (ion-nucleus, ion-electron, electron-electron, and Bremsstrahlung radiation loss of electron) are indicated. Right panel: total energy loss per pathlength for different atoms.

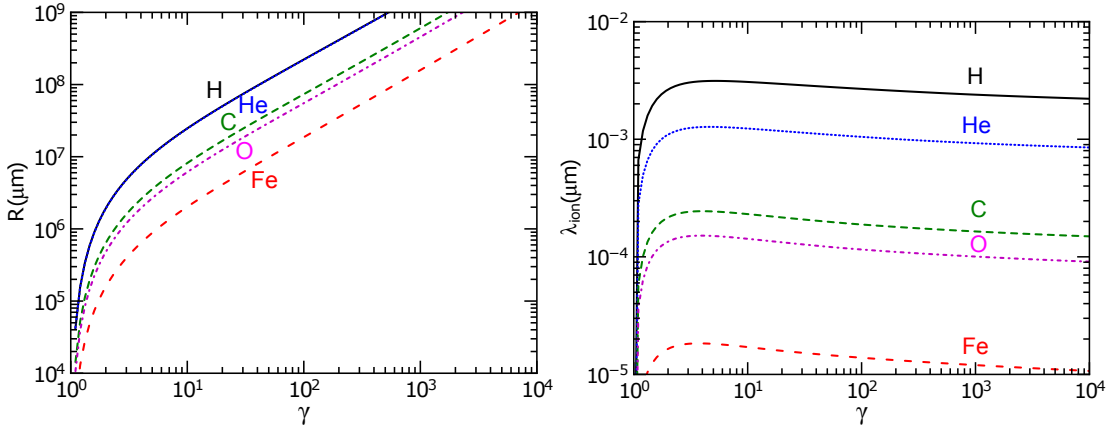


FIG. 4.— Range R (left) and mean ionization length λ_{ion} (right) for different ions in silicate material with $W = 8 \text{ eV}$.

for small ($a \sim 0.01 \mu\text{m}$) grains with $E > 100 \text{ eV}$, an important fraction of photon energy is carried away by free photoelectrons, while for larger grains ($a > 0.1 \mu\text{m}$), most of photon energy with $E < 10^3 \text{ eV}$ is deposited to the grain.

5.3. Grain equilibrium temperature

The heating rate by radiation field for a spherical grain of size a , in general, depends on the specific spectral energy flux of photons $cu(\nu', \mu')$ coming from the direction μ' , the absorption cross-section $Q_{\text{abs}}(\nu', a)$, and the fraction of photon energy deposited to the grain $f_{\text{dep}}(\nu')$, which is described by

$$\frac{dE_h}{dt'} = \int d\nu' \int d\mu' \pi a^2 Q_{\text{abs}}(\nu', a) f_{\text{dep}}(\nu') cu(\nu', \mu'), \quad (42)$$

where ν' denotes the photon frequency in the GF.

For the point source of the solar radiation field, the photon frequency in the GF is $\nu' = \nu\gamma(1 + \beta)$, assuming that the dust grain is coming to the Sun in the radial direction ($\mu_{\text{gr}} = -1$). Using the transformations for μ', ν' and $u'(\nu', \mu')$ versus μ, ν and $u(\nu, \mu)$ in Section 3, the integral over μ can be analytically carried out and one obtains:

$$\frac{dE_h}{dt'} = \int d\nu \pi a^2 Q_{\text{abs}}(\nu', a) f_{\text{dep}}(\nu') cu(\nu) \gamma^2 (1 + \beta)^2. \quad (43)$$

For the isotropic radiation (e.g., ISRF, CMB), the photon frequency in the GF is a function of both photon frequency in the SF and its incoming direction as $\nu' = \nu\gamma(1 - \beta\mu)$. Using the transformations in Section 3, the integral can be rewritten as

$$\frac{dE_h}{dt'} = \int d\nu \int_{-1}^1 d\mu \pi a^2 Q_{\text{abs}}(\nu', a) f_{\text{dep}}(\nu') c \frac{u(\nu)}{2} \gamma^2 (1 - \beta\mu)^2, \quad (44)$$

where the term $(1 - \beta\mu)^2$ describes the focusing effect of radiation due to the relativistic motion of the grain. Since ν' is a function of μ , we integrate numerically the integral over μ using a grid of 32 directions for μ .

The grain isotropically emits thermal radiation with a cooling rate:

$$\begin{aligned} \frac{dE_c}{dt'} &= \int d\nu' 4\pi a^2 Q_{\text{abs}}(\nu', a) B(\nu', T_d), \\ &= 4\pi a^2 \langle Q_{\text{abs}}(T_d) \rangle \sigma T_d^4, \end{aligned} \quad (45)$$

where T_d is the grain equilibrium temperature and $\langle Q_{\text{abs}}(T_d) \rangle = \int d\nu' Q_{\text{abs}}(\nu', a) B(\nu', T_d) / \int d\nu' B(\nu', T_d)$ is the Planck-averaged absorption efficiency.

To find T_d , we solve the equation $dE_h/dt' + dE_{\text{coll}}/dt' = dE_c/dt'$ numerically with the use of Q_{abs} computed from the previous section and f_{dep} from Dwek & Smith (1996).

Heating and cooling appears to be fast such that the

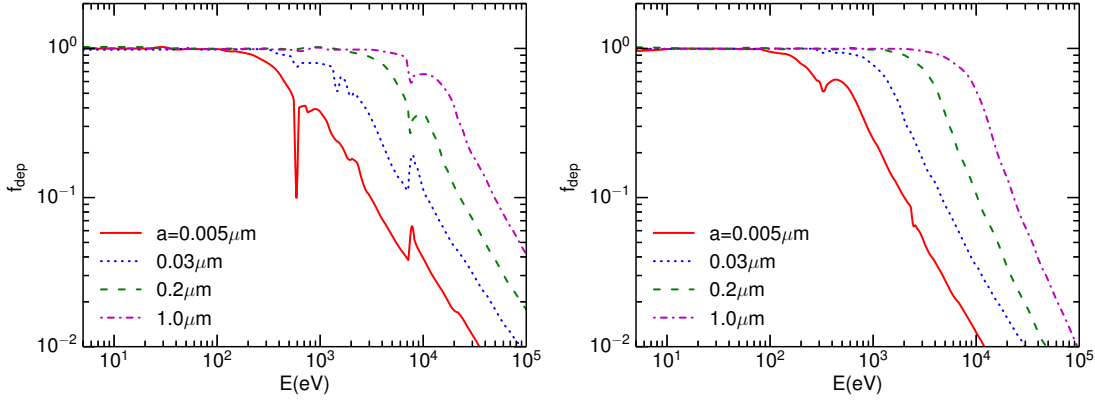


FIG. 5.— Fraction of photon energy deposited to the grain f_{dep} as a function of the photon energy for silicate (left) and carbonaceous grains (right). Different grain sizes are considered. f_{dep} declines rapidly for $E > 10^2 - 10^3$ eV. Data are taken from [Dwek & Smith \(1996\)](#).

effect of grain motion toward the Sun on the grain equilibrium temperature is disregarded, i.e., the motion time that considerably increases grain temperature is longer than the time needed for the grain to achieve thermal equilibrium. Thus, the grain temperature can be calculated for arbitrary distance r from the Sun. First, we assume that the solar radiation field can be approximated as a monochromatic radiation field with photon energy equal to the averaged energy $h\nu_{\odot} \approx 2.7k_{\text{B}}T_{\odot} = 1.34$ eV. The photon energy $h\nu'$ and energy density $u'(\nu')$ in the GF are obtained through the transformations in Section 3.

The grain equilibrium temperature is calculated for two limiting cases. In the first case, we assume $f_{\text{dep}} = 1$, i.e., entire photon energy is transferred to the grain heat. In the second case, we take the energy-dependence f_{dep} from [Dwek & Smith \(1996\)](#) computed for neutral grains. These two limiting cases would provide upper and lower bounds for the grain temperature.⁶

Figure 6 shows the equilibrium temperature for silicate grains of different sizes at $r = 1$ AU for $f_{\text{dep}} = 1$ (left) and photon energy-dependence f_{dep} (right). In the first case, T_d tends to increase with increasing γ and achieves a stable value $T_d \sim 10^4$ K for $\gamma > 10^3$. In the second case, T_d increases with γ until $\gamma = 10^3$ then starts to decline for $\gamma > 10^3$. The decline of T_d at high γ that is more important for smaller grains is a direct consequence of the decrease of f_{dep} to a value below unity for $E > 10^3$ eV (see Figure 5).

Figure 7 shows the dust temperature calculated for silicate and graphite grains with the photon energy-dependence f_{dep} and for full spectrum of solar radiation. Spectral features seen in Figure 6 are averaged out so that the temperature is a smooth function of γ .

5.4. Melting and Sublimation of Relativistic Dust

5.4.1. Melting

Dust grains will melt when heated above the melting temperature T_m . Silicate grains containing irons are assumed to have $T_m = 1800$ K, whereas graphite grains made of carbons can have a high melting temperature up to $T_m = 4000$ K ([Savvatimskiy 2005](#)).

⁶ The effect of positive grain charge is expected to increase f_{dep} because photoelectrons must overcome a higher potential barrier than in the case of neutral grain to escape from the grain surface.

From Figure 7, it can be seen that the silicate grains moving with $\gamma > 10$ have already melt, while the grains with $\gamma < 10$ may survive. Similarly, graphite grains with $\gamma > 100$ have already melted if a high melting temperature $T_m = 4000$ K is adopted.

It is also useful to know at what solar distance the grain's melt occurs. To this end, we find the grain temperature for different distances $T_d(r)$ and infer the melting distance using $R_m \equiv r(T_d = T_m)$. Figure 8 shows the contours of R_m in the plane of γ, a for silicate and graphite grains of different sizes.

5.4.2. Sublimation

Since the melting temperature of graphite is rather high. The sublimation is expected to be important for $T_d < T_m$. Moreover, grains would sublimate rapidly when $T_d = T_m$, but whether grains can survive depend on their life time before completely destroyed by sublimation and the arrival time into the Earth atmosphere.

[Guhathakurta & Draine \(1989\)](#) investigated the sublimation assuming thermal equilibrium, i.e., evaporation of atoms from the grain surface is balanced by sticking collisions of incident atoms from the gas. In the case of relativistic dust, gaseous atoms likely pass through the grain (see Section 4), thus, the sublimation is considered to be the evaporation of atoms from the grain surface into vacuum. For rough estimates, we adopt the sublimation rate from [Guhathakurta & Draine \(1989\)](#) as follows:

$$\frac{da}{dt'} = - \left(\frac{m}{\rho} \right)^{1/3} \nu_0 \exp \left(\frac{-B}{k_{\text{B}}T_d} \right), \quad (46)$$

where $\nu_0 = 2 \times 10^{15}$ s and $B/k_{\text{B}} = 68100$ K for silicate grains, $\nu_0 = 2 \times 10^{14}$ s and $B/k_{\text{B}} = 81200$ K for carbonaceous grains, and m is the average atomic mass of dust ([Guhathakurta & Draine 1989](#); [Waxman & Draine 2000](#)).

The sublimation time of a dust grain with size a in the SF can be defined as

$$\tau_{\text{sub}}(T_d) = -\gamma \frac{a}{da/dt'}, \quad (47)$$

$$= a\gamma \left(\frac{\rho}{m} \right)^{1/3} \nu_0^{-1} \exp \left(\frac{B}{k_{\text{B}}T_d} \right). \quad (48)$$

Plugging the numerical parameters into the above

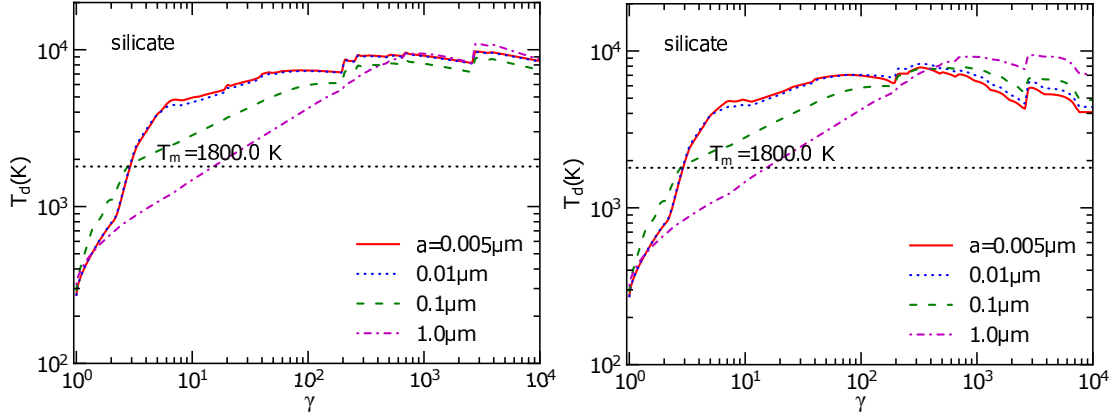


FIG. 6.— Equilibrium temperature of silicate grains at distance 1 AU from the Sun as a function of the Lorentz factor γ obtained for $f_{\text{dep}} = 1$ (left) and energy-dependence f_{dep} (right). Monochromatic approximation of the solar radiation field is assumed. Averaged energy of the solar photon in the GF is $h\bar{\nu}'_{\odot} = 2\gamma h\bar{\nu}_{\odot} \approx 2.7\gamma \text{ eV}$. Spikes in T_d are produced by absorption features of silicate grains. Melting temperature for silicate $T_m = 1800 \text{ K}$ is indicated, and grains melt for $T_d \geq T_m$.

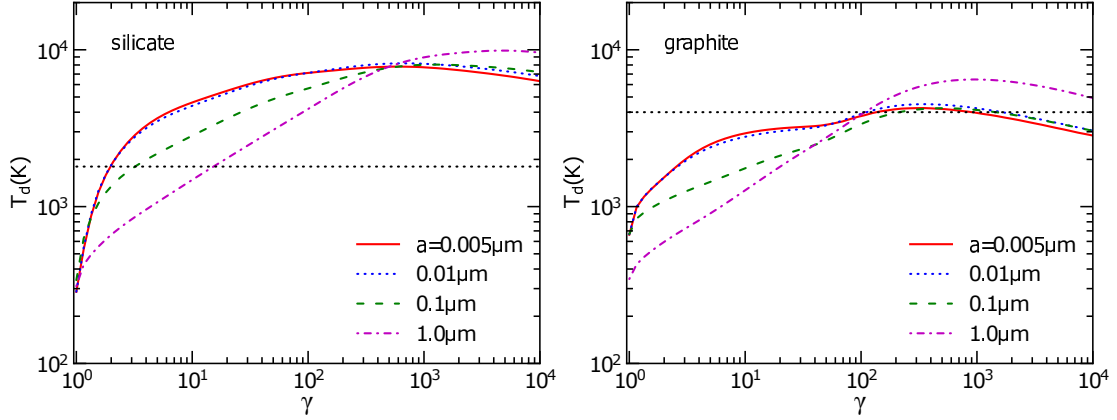


FIG. 7.— Same as Figure 6 but for the full spectrum of the solar radiation field. Horizontal dotted lines show the melting temperature, $T_m = 1800 \text{ K}$ for silicate grains and $T_m = 4000 \text{ K}$ for graphite grains. Silicate grains of $a \sim 1 \mu\text{m}$ with $\gamma < 10$ and most graphite grains with $\gamma < 100$ will survive the melting.

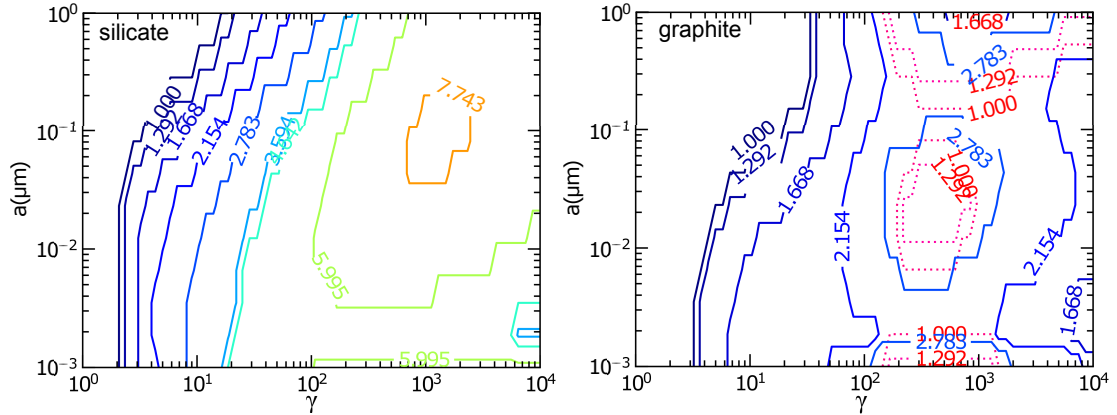


FIG. 8.— Left panel: contours of melting distance R_m measured in AU in the plane of γ, a for silicate grains. Right panel: contours of R_m for graphite grain. Solid and dotted contours show results for $T_m = 2000 \text{ K}$ and $T_m = 4000 \text{ K}$. Grains with lower γ melt at smaller distance R_m and will survive the melting for $R_m \leq 1 \text{ AU}$.

equation, we obtain

$$\tau_{\text{sub}}(T_d) = 6.36 \times 10^3 \gamma a_{-5} \exp \left[68100 \text{ K} \left(\frac{1}{T_d} - \frac{1}{1800 \text{ K}} \right) \right] \quad (49)$$

for silicate grains, and

$$\tau_{\text{sub}}(T_d) = 1.36 a_{-5} \gamma \exp \left[81200 \text{ K} \left(\frac{1}{T_d} - \frac{1}{3000 \text{ K}} \right) \right] \quad (50)$$

for graphite grains.

It can be seen that the sublimation time of silicate grains with $T_d \sim 1800 \text{ K}$ is sufficiently long compared to the time needed to reach the Earth $\tau_{\text{arr}} = (R_m - 1 \text{ AU})/(\beta c) = 500 \text{ s}$ for $R_m = 2 \text{ AU}$ and $\beta \sim 1$. As a result, the relativistic grains that survive the melting at $R_m \leq 2 \text{ AU}$ can enter the Earth atmosphere as UHE-CRs.

To see the survival of grains that melt at $R_m > 2 \text{ AU}$ while approaching us, we integrate Equation (46) to get the grain size at $r_f = 1 \text{ AU}$:

$$a_f - a_i = \int_{r_i}^{1 \text{ AU}} \left(\frac{m}{\rho} \right)^{1/3} \nu_0 \exp \left(-\frac{B}{k_B T_d(r)} \right) \frac{dR}{\beta c}, \quad (51)$$

where the increase of T_d with decreasing r is included. We characterize the decrease of grain size from initial size a_i to final a_f at 1 AU as follows:

$$\frac{\delta a_{\text{sub}}}{a} = \frac{a_i - a_f}{a_i}. \quad (52)$$

The obtained results $\delta a_{\text{sub}}/a$ are shown in Figure 9 for silicate (left) and graphite (right) grains. There appears to exist a survival window of relativistic grains with parameters (a, γ) satisfying $\delta a_{\text{sub}}/a < 0.1$ (blue areas). Grains are said to be completely destroyed for $\delta a_{\text{sub}}/a = 1$. For graphite grains, there exists two regions of survival at low ($\gamma < 100$) and high γ ($\gamma > 10^3$). The latter arises from the decrease of $f_{\text{dep}} < 1$ at highest photon energy.

6. CHARGING OF RELATIVISTIC GRAINS IN THE SOLAR RADIATION FIELD

6.1. Collisional charging

In the high-energy regime (i.e., above GeV for ions and MeV for electrons), incident electrons and ions have the range R much larger than the grain size (see Figure 3). Therefore, they do not stick to the grain to build up grain charge as in the low-energy regime. Nevertheless, as discussed in Section 4, considerable energy acquired from heavy (e.g., Fe) ions during collisions can allow target atoms to emit a large number of photoelectrons in a track along the ion path. Such photoelectrons of low energy ($E < \Delta E_1 \sim 130 \text{ eV}$) quickly transfer their energy to nearby atoms. Therefore, these photoelectrons are potentially not energetic enough to overcome the Coulomb surface barrier in the case grains are positively charged by photoelectric emission in the strong solar radiation field. Although the sputtering effect can eject some ions (i.e., surface potential) from the grain, we will see in Section 7 that this process is relatively inefficient in the high-energy regime. Therefore, collisional charging by ions and electrons from the diffuse medium appears to be minor and can be disregarded for relativistic dust.

6.2. Photoelectric Emission

Following the absorption of an energetic photon, a relativistic grain becomes positively charged as a result of three basic processes: emission of primary photoelectrons, emission of Auger electrons, and emission of secondary electrons excited by high-energy primary photoelectrons and Auger electrons. A detailed description of photoelectric emission from dust by X-ray is presented in Weingartner et al. (2006). Here we adopt the same notations and present principal formula needed for our calculations.

Let Y_{pe} , Y_{A} and Y_{sec} be the photoelectric yields for primary, Auger, and secondary electrons, which are functions of photon energy $h\nu'$, grain size a , and grain charge Z . Detailed expressions for the photoelectric yields are summarized in Appendix C.1.

The charging rate by photoelectric emission depends in general on the absorption cross-section, photoelectric yield, and the flux of incident photons, which is given by

$$J_{\text{pe}}(a, Z) = \int_{\nu_{\text{pet},b}}^{\nu'_{\text{max}}} d\nu' \int_{-1}^1 d\mu' \pi a^2 Q_{\text{abs}} \left[Y_{p;b} + \sum_{i,s} Y_{p;i,s} \right] cn', \quad (53)$$

where ν' is the frequency and $n' = n'(\nu', \mu')$ is the density of photons coming from direction μ' in the GF, $\nu_{\text{pet},b}$ denotes the frequency threshold of photoelectric emission from the band structure (see Appendix C.1), and ν'_{max} is the maximum frequency of the radiation spectrum in the GF. Here, $Y_{p;b}$ is the yield of primary photoelectrons from the band structure, $Y_{p;i,s}$ is the partial yield from electronic shell s of element i (see Table 1), and the sum is taken over all inner shells s and elements i . In addition, the dependence of Q_{abs} and Y on ν' have been omitted for simplicity.

The charging rate due to the emission of Auger electrons is equal to

$$J_{\text{A}}(a, Z) = \int_{I_{is,\min}/h}^{\nu'_{\text{max}}} d\nu' \int_{-1}^1 d\mu' \pi a^2 Q_{\text{abs}} \sum_{i,s,j} Y_{A;i,s,j} cn', \quad (54)$$

where $I_{is,\min}$ is the ionization potential of the shell is , and the sum is over all electronic shells s , elements i , and Auger transitions j .

Similarly, the charging rate for secondary effects arising from the excitation of primary photoelectrons and Auger electrons is equal to

$$J_{\text{sec}}(a, Z) = \int_{\nu_{\text{pet},b}}^{\nu'_{\text{max}}} d\nu' \int_{-1}^1 d\mu' \pi a^2 Q_{\text{abs}} \sum_k Y_{\text{sec};k} cn', \quad (55)$$

where the sum runs over all primary photoelectrons and Auger electrons. In the above equations, the dependence of Q_{abs} on (ν', a) and of Y on $(h\nu', a, Z)$ is omitted.

For the point source of radiation (e.g., solar radiation), using the transformations from μ', ν' and $n'(\nu', \mu')$ to μ, ν and $n(\nu, \mu)$ presented in Section 3 and carrying out integration over μ , the charging rate due to photoelectric emission can be simplified as:

$$J_{\text{chrg}}(a, Z) = \int d\nu \pi a^2 Q_{\text{abs}} Y_{\text{chrg}} c \frac{u(\nu)}{h\nu} \gamma (1 + \beta), \quad (56)$$

where chrg denotes pe, A, or sec, pe process.

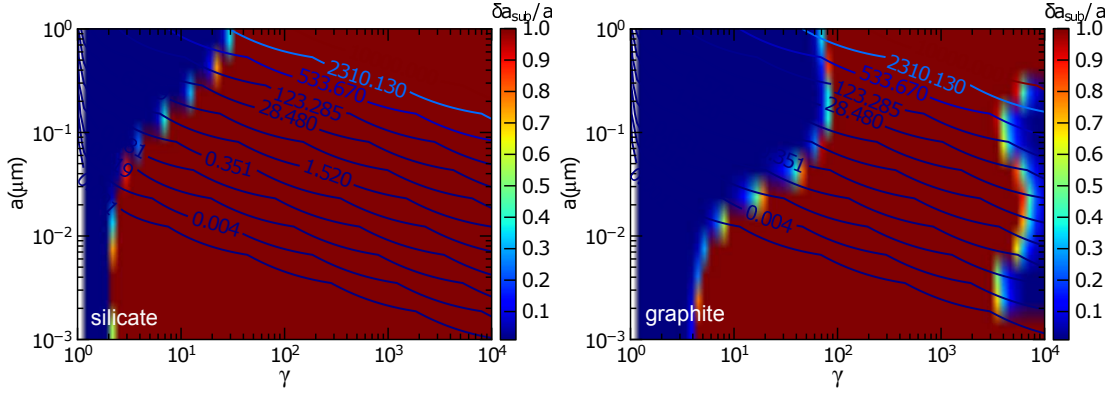


FIG. 9.— Map of $\delta a_{\text{sub}}/a$ at 1 AU in the plane (γ, a) for silicate (left panel) and graphite (right panel). Regions with $\delta a_{\text{sub}}/a \geq 0.1$ indicate grain sublimation is significant, and the regions with $\delta a_{\text{sub}}/a = 1$ correspond to the complete destruction of grains. Contours show the levels of grain kinetic energy E_{gr} in units of 10^{20} eV.

For the case of isotropic radiation, the photon frequency in the GF, ν' , depends on both ν and μ , so the charging rate can be rewritten as

$$J_{\text{chrg}}(a, Z) = \int d\nu \int_{-1}^1 d\mu \pi a^2 Q_{\text{abs}} Y_{\text{chrg}} c \frac{u(\nu)}{2h\nu} \gamma (1 - \beta\mu). \quad (57)$$

The total charging rate due to photoelectric emission in the GF is then given by

$$\frac{dZ(a, Z)}{dt'} \equiv J_{\text{tot}}(a, Z), \quad (58)$$

where

$$J_{\text{tot}}(a, Z) = J_{\text{pe}}(a, Z) + J_{\text{A}}(a, Z) + J_{\text{sec}}(a, Z). \quad (59)$$

6.3. Maximum grain charge

6.3.1. Coulomb explosions

The emission of photoelectrons increases grain charge rapidly with time if photon energy is above the photoelectric threshold. This results in an increased electric potential $\phi = Ze/a$ and tensile strength $\mathcal{S} = (\phi/a)^2/4\pi$, accordingly. When the tensile strength exceeds the maximum limit that the material can support \mathcal{S}_{max} , the grain will be disrupted by Coulomb explosions.

Setting $\mathcal{S} = \mathcal{S}_{\text{max}}$, we can derive the maximum potential and charge that the grain still survives as the followings:

$$\phi_{\text{max}} = 1.06 \times 10^3 \left(\frac{\mathcal{S}_{\text{max}}}{10^{10} \text{ dyn cm}^{-2}} \right)^{1/2} a_{-5} V, \quad (60)$$

$$Z_{\text{max}} = 7.4 \times 10^4 \left(\frac{\mathcal{S}_{\text{max}}}{10^{10} \text{ dyn cm}^{-2}} \right)^{1/2} a_{-5}^2. \quad (61)$$

The maximum tensile strength \mathcal{S}_{max} is uncertain due to the uncertainty in grain material. Measurements for ideal material provide $\mathcal{S}_{\text{max}} = 10^{11} \text{ dyn cm}^{-2}$. Here we take a typical material $\mathcal{S}_{\text{max}} \sim 10^{10} \text{ dyn cm}^{-2}$ for our numerical considerations.

6.3.2. Ion field emission

When a grain is positively charged to a sufficiently strong electric field, the emission of individual ions (ion field emission) from the grain surface can take place. Experiments show that with an electric field $\phi/a \approx 3 \times 10^8 \text{ V cm}^{-1}$, ion field emission already occurs for some

metals (see Table 1 in Tsong & Müller 1970). Thus, grains may be destroyed by ion field emission before Coulomb explosions in the case of ideal material with $\mathcal{S}_{\text{max}} \sim 10^{11} \text{ dyn cm}^{-2}$. For the typical \mathcal{S}_{max} adopted, the maximum grain potential is determined by Equation (60).

6.4. Results for photoelectric yield

To solve Equation (58) for grain charge, we first need to know the photoelectric yields. To this end, we follow the approaches in Weingartner et al. (2006) for high-energy photons ($E > 50 \text{ eV}$) and in Weingartner & Draine (2001) for low-energy photon ($E < 20 \text{ eV}$). For $20 \text{ eV} < E < 50 \text{ eV}$, we interpolate between two ranges. We assume that silicate material is made of MgFeSiO_4 , while graphite material purely consists of carbons. The mass density is $\rho = 3.5 \text{ g cm}^{-3}$ and 2.2 g cm^{-3} for silicate and graphite, respectively. The ionization potentials $I_{i,s}$ for different shells and elements are listed in Table 1. The energy and averaged number of Auger electrons following a primary transition are taken from Table 4.1 and 4.2 in Dwek & Smith (1996).

Figure 10 (left) shows the total photoelectric yield (sum over the yields of primary photoelectrons, Auger and secondary electrons) for a neutral silicate grain of different sizes. The yield tends to increase with increasing photon energy for $E > 50 \text{ eV}$ and becomes flat at very high energy. Also, the yield is higher for smaller grains and can be more than unity (i.e., one energetic photon can produce more than one free electron).

Figure 10 (right) shows the results for a carbonaceous grain. For $a \geq 0.01 \mu\text{m}$ grains, as shown, Y increases first from $E = 10 \text{ eV}$ to about 20 eV . Then, it declines rapidly until $E \sim 50 \text{ eV}$ where the secondary effect becomes important. For $E > 50 \text{ eV}$, the emission of secondary electrons becomes important and Y start to rise. When $E \sim 291.01 \text{ eV}$ —the energy sufficient to excite K-shell electrons in C atoms and to produce Auger electrons — Y starts to rise sharply with the increased E .

Figure 11 shows the photoelectric yield computed for a grain of charge $Z = Z_{\text{max}}$ given by Equation (61). The yield Y tends to zero when the photon energy becomes lower than the ionization potential $\text{IP}(Z = Z_{\text{max}})$. Moreover, for photon energy higher than $\text{IP}(Z_{\text{max}})$, Y is also decreased compared to that for the neutral grain due to the higher potential ionization.

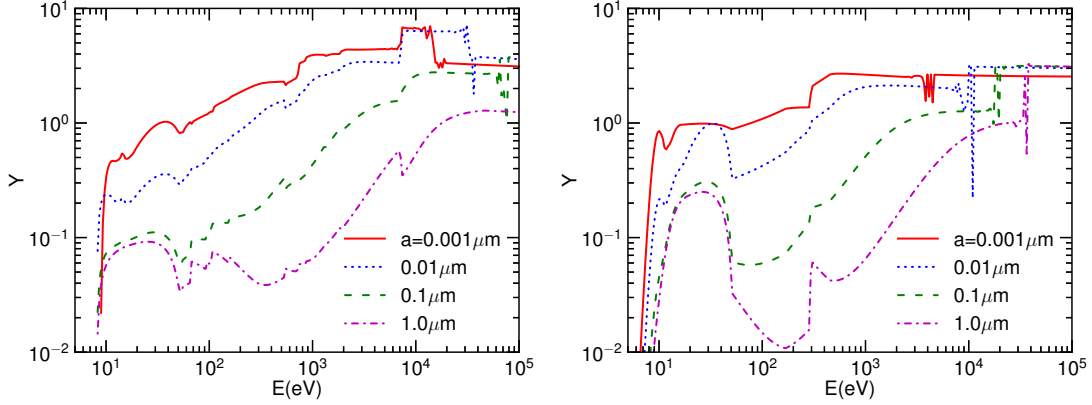


FIG. 10.— Total photoelectric yield due to the emission of primary, Auger and secondary electrons as a function of photon energy for silicate (left) and graphite (right). Neutral grains ($Z = 0$) and different grain sizes are considered.

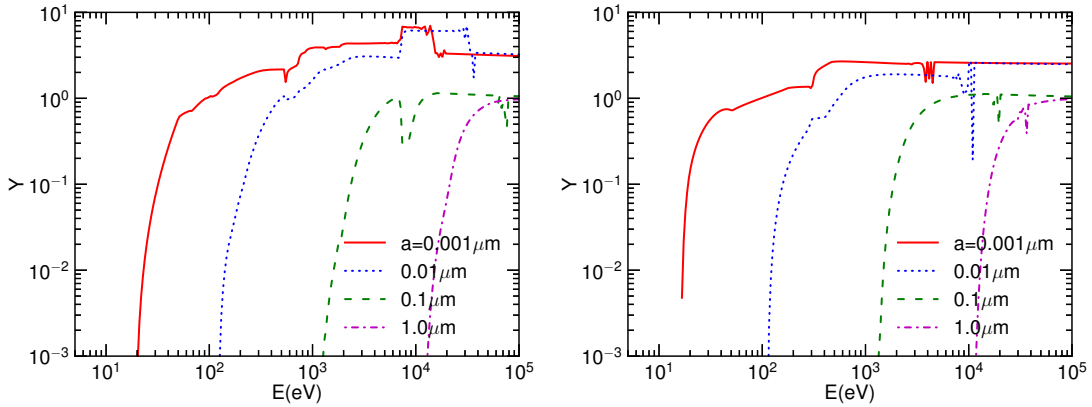


FIG. 11.— The same as Figure 10 but for grains with $Z = Z_{\max}$. The yield for the low-energy part is significantly suppressed due to the increased potential barrier determined by Z_{\max} .

6.5. Coulomb explosions by the solar radiation field

Now we calculate the charging rate and the maximum charge accumulated for a relativistic grain entering our solar system. Here we consider its full spectrum of solar radiation given by the Planck function $B(\nu, T_{\odot})$. The photon energy $h\nu'$ and spectral energy density $u'(\nu')$ in the GF are obtained through the transformations in Section 3.

Since the density of solar photons decreases with distance as $n \propto 1/r^2$, we can rewrite the charging rate (Eq. 58) as the following

$$\frac{dZ}{dt'} = J_{\text{tot}}(a, Z)|_{\text{AU}} \left(\frac{\text{AU}}{r} \right)^2, \quad (62)$$

where $J_{\text{tot}}(a, Z)|_{\text{AU}}$ is the charging rate calculated at distance $r = 1 \text{ AU}$.

Thus,

$$\frac{dZ}{J_{\text{tot}}(a, Z)|_{\text{AU}}} = \text{AU}^2 \frac{dt'}{r^2} = \frac{\text{AU}^2}{\gamma \beta c} \frac{dr}{r^2}, \quad (63)$$

where $dr = \beta c dt = \beta \gamma dt'$ has been used.

To determine the final distance at $Z = Z_{\max}$, we integrate the above equation from $Z = Z_i$ to $Z = Z_{\max}$, which correspond to $r = R_i$ to $r = R_{\max}$. It yields

$$\left(\frac{1}{R_{\max}} - \frac{1}{R_i} \right) = \frac{\gamma \beta c}{\text{AU}^2} \times \int_{Z_i}^{Z_{\max}} \frac{dZ}{J_{\text{tot}}(a, Z)|_{\text{AU}}}. \quad (64)$$

It is valid to assume $R_i \gg R_{\max}$ and $Z_i = 0$ without resulting in considerable differences, because Z_{\max} is much larger than the average equilibrium charge of the interstellar grains. Thus, one obtains

$$R_{\max} = \frac{\text{AU}^2}{\gamma \beta c} \times \left[\int_0^{Z_{\max}} \frac{dZ}{J_{\text{tot}}(a, Z)|_{\text{AU}}} \right]^{-1}. \quad (65)$$

As shown, R_{\max} is determined by the integral of $1/J_{\text{tot}}(a, Z)|_{\text{AU}}$. To obtain $J_{\text{tot}}(a, Z)|_{\text{AU}}$, we first need to compute the photoelectric yield $Y_{\text{pe}}(a, Z)$ for $Z = 0$ to $Z = Z_{\max}$, which is the most time consuming part of the numerical integration.

Figure 12 shows the obtained results for R_{\max} as a function of γ for different grain sizes. As shown, some grains can reach the Earth atmosphere ($R_{\max} < 1 \text{ AU}$). For instance, the $a = 0.1 \mu\text{m}$ grains with $\gamma < 10^2$ can reach the Earth. Similarly, the $1 \mu\text{m}$ grains with $\gamma < 10^3$ would survive Coulomb explosions but be destroyed for $\gamma > 10^3$. For all grain sizes considered, R_{\max} tends to fall after reaching its peak, which directly arises from the decrease of Q_{abs} at highest photon energy (see Figure 2) that decreases the charging rate.

For relativistic grains with $\gamma > 10^4$, the charging rate is calculated using the Compton theory (see Appendix C). The grain charge at distance $r = 1 \text{ AU}$ is estimated

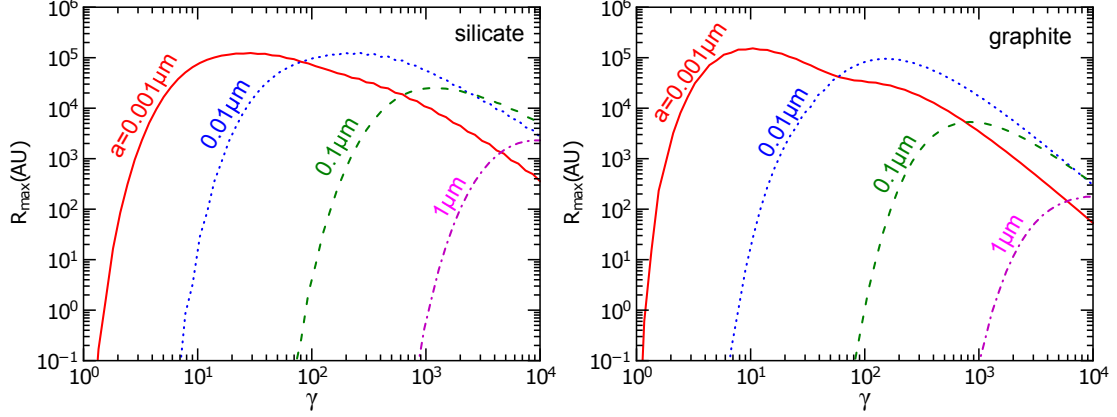


FIG. 12.— Distance R_{\max} from the Sun that a relativistic grain is electrically charged to Z_{\max} from $Z = 0$ at infinity, for silicate grains (left) and graphite grains (right panel). Typical maximum tensile strength $S_{\max} = 10^{10} \text{ dyn cm}^{-2}$ is adopted. All grains with $\gamma > 10^3$ explode at a large distance from the Sun in the solar radiation field, while some relativistic grains with lower γ can reach the Earth atmosphere.

to be:

$$Z_C(r = 1 \text{ AU}) = 8.8 \times 10^{10} \left(\frac{\text{AU}}{c\beta} \right) a_{-5}^3 \exp \left(-\frac{0.4a_{-5}^{1/4} \hat{\rho}^{1/4}}{\gamma_5} \right),$$

$$= 4.4 \times 10^{13} a_{-5}^3 \beta^{-1} \exp \left(-\frac{0.4a_{-5}^{1/4} \hat{\rho}^{1/4}}{\gamma_5} \right). \quad (66)$$

Comparing $Z_C(r = 1 \text{ AU})$ and Z_{\max} it can be seen that relativistic grains with $\gamma > 10^4$ are easily destroyed by Coulomb explosions in the Solar radiation field.

7. DESTRUCTION OF RELATIVISTIC GRAIN BY INTERSTELLAR GAS AND DUST

7.1. Introduction to Electronic Sputtering

The ejection of atoms from interstellar dust by shocks in the low-energy regime has been well studied (Draine & Salpeter 1979a; Tielens et al. 1994). This *knock-on* sputtering arises from elastic collisions between incident ions and atomic nuclei of the dust grain in which the kinetic energy of incident ions is directly converted to atomic motion (Sigmund 1981). When the velocity of incident ions is larger than the Bohr velocity v_0 (high-energy regime), electronic interactions become essential and electronic sputtering has been studied extensively both numerical simulations and experiments. Two models have been suggested to explain electronic sputtering, including *thermal spike* model and *Coulomb explosion* model (see Johnson & Schou 1993 and Bringa & Johnson 2003 for reviews).

In the *thermal spike* model, electronic sputtering is believed to occur as the following. After the passage of a swift heavy ion, on a timescale $t \sim 10^{-17} - 10^{-13} \text{ s}$, electronic excitations and ionizations occur, producing secondary electrons in a narrow cylindrical track along the ion's path through the grain. In $10^{-13} - 10^{-11} \text{ s}$, secondary electrons (of energy typically between 1-100 eV) rapidly transfer their energy to surrounding atoms, producing a hot cylinder (hot spot) of radius of $\sim 10 \text{ \AA}$. Some highly excited atoms in the hot cylinder (near surface) can gain sufficient energy to break atomic bonds and escape from the grain surface (sputtering). In $10^{-9} - 10^{-5} \text{ s}$, the grain temperature becomes uniform throughout the grain.

In the *Coulomb explosion* model, electrostatic repulsion between transiently ionized atoms in the ionization track (Fleischer et al. 1965) directly converts electrostatic energy to atomic motion, which can result in the ejection of atoms near the grain surface (Johnson & Brown 1982). In both models, the presence and characteristics of the ionization track are a key factor for interpreting electronic sputtering.⁷

7.2. Track Radius and Sputtering Yield

7.2.1. Track Radius

The radius of the ionization track (hot cylinder) created by an energetic heavy ion, r_{cyl} , can be calculated using the bond-braking model (Tombrello 1994):

$$r_{\text{cyl}} = \left(\frac{\eta}{2\pi e_c} \frac{dE}{dx} \right)^{1/(2-\eta)} R_{\perp}^{\eta/(2-\eta)}, \quad (67)$$

where e_c is the critical energy density for bond braking, $0 < \eta < 1$ is a constant obtained from fitting to experimental data, and $R_{\perp} = (840\epsilon/\rho) \text{ \AA}$ is the maximum radial range of secondary electrons in the material with ϵ being the ion energy in units of MeV/u ($u = 931.5 \text{ MeV}$).

The track radius obtained from Equation (67) was found in good agreement with the experimental data (see e.g., Bringa et al. 2007). For our calculations for silicate grains, we use the good fit parameters from Tombrello (1994) $e_c = 0.024 \text{ eV \AA}^{-3}$ and $\eta = 0.27$ for Fe ion bombarding SiO_2 . For carbonaceous grains, we adopt $e_c = 0.014 \text{ eV \AA}^{-3}$ for polystyrene (C_8H_8).

All atoms in the hot cylinder of height l are excited, and it is useful to define an average excitation energy per atom as follows:

$$E_{\text{exc}} = \frac{ldE/dx}{n_d l \pi r_{\text{cyl}}^2} = \frac{dE/dx}{n_d \pi r_{\text{cyl}}^2}, \quad (68)$$

where n_d is the atomic number density in the grain.

Light energetic ions (H, He) have low dE/dx and can only create a few ionizations along the entire track in the

⁷ It was noted that the thermal spike model was numerically shown to be important while the Coulomb explosion is dominant in the early stage $t < 0.2\tau_D$ with $\tau_D \sim 10^{-13} \text{ s}$ heat diffusion time and at highest excitation density (Bringa & Johnson 2002).

grain. In this case, r_{cyl} given by Equation (67) may be smaller than $l/2$, which results in high E_{exc} even the heated cylinder is narrower than the interatomic distance. Therefore, E_{exc} should be taken to be ΔE_1 from Equation (39).

7.2.2. Electronic Sputtering Regimes

Let U be the binding energy of the grain material and $Y_{\text{sp},i}$ be the sputtering yield induced by incident ion i . Depending on the ratio of E_{exc} to U , different regimes of electronic sputtering are reported in both experiments and molecular dynamic simulations. In the case $E_{\text{exc}} > U$, namely *high-excitation energy* regime, the yield is found to have a quadratic dependence on dE/dx (Johnson et al. 1991; Matsunami et al. 2002). In the case $E_{\text{exc}} < U$, so-called *low-excitation energy* regime, the yield depends nonlinearly on dE/dx (see e.g., Urbassek et al. 1994 for simulations and Matsunami et al. 2003 for experiments).

In the *high-excitation energy* regime, all atoms in the heated cylinder of radius r_{cyl} are excited, and the sputtering yield can be written as the following (see Bringa & Johnson 2000):

$$Y_{\text{sp},i} = C_{\text{high}} \left(\frac{r_{\text{cyl}} dE/dx}{U} \right), \quad (69)$$

where C_{high} is a coefficient which describes the fraction of dE/dx converted to atomic motion and the effects of incident angle of ions for this high-excitation regime. Due to the increase of r_{cyl} with dE/dx , Equation 69 was found to successfully explain the quadratic dependence of Y on dE/dx for sputtering by He and H on solid O_2 in Bringa & Johnson (2000). Later on, it is used to describe the sputtering by energetic Fe ions from volatile ice in (Bringa & Johnson 2004).

In the *low-excitation energy* regime, the sputtering yield can be described by

$$Y_{\text{sp},i} = C_{\text{low}} \left(\frac{f l dE/dx}{U} \right)^q, \quad (70)$$

where f is the fraction of dE/dx converted to atomic motion, C_{low} is a coefficient for this low-excitation regime, and $q \geq 3$ (see Matsunami et al. 2002 and Matsunami et al. 2007 for experiments, and see Urbassek et al. 1994, Bringa et al. 1999a, and Bringa et al. 1999b for simulations).

7.2.3. Sputtering Yield: Experimental Data and Calculations

Figure 13 shows the sputtering yield as a function of dE/dx for SiO_2 from experiments Matsunami et al. (2002) and yield computed for Fe ion using Equation (69) with $C_{\text{high}} = 0.02$ (solid line) and Equation (70) with $C_{\text{low}} = 0.02$, $f = 0.05$ and $q = 3.3$ (dashed line). We can see that Equation (69) for the high-excitation energy regime fits well to the experimental data for $dE/dx > 8 \times 10^{10} \text{ eV cm}^{-1}$. For lower energy loss dE/dx , the experimental data are better fitted with the yields calculated for the low-excitation energy (threshold regime).

The figure also shows the experimental results from Khan et al. (2013) for graphite grains. For the same

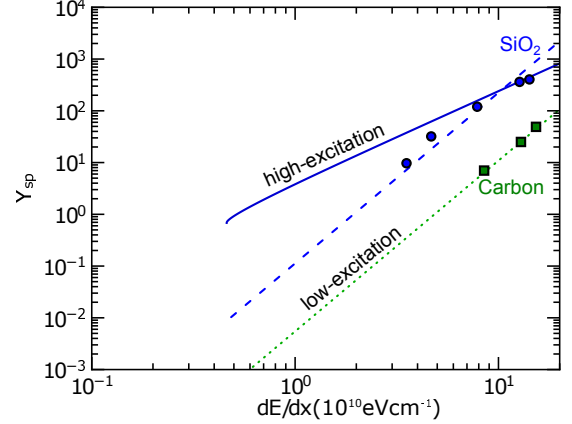


FIG. 13.— Electronic sputtering yield Y_{sp} vs. stopping power dE/dx for SiO_2 (filled circles) and graphite (carbon solid). Calculations using the high- and low-excitation energy models are shown in solid and dashed lines for SiO_2 . Dotted line shows calculations for graphite using the low-excitation energy model.

dE/dx , the yield is significantly lower than that for SiO_2 and can be well described by the yield computed from the threshold regime with $C_{\text{low}} = 0.005$, $f = 0.02$ and $q = 3.3$ (dotted line). The lower f value required to fit the data for graphite perhaps is due to its high conductivity for which photoelectron energy is rapidly transferred to the entire grain rather than being localized within the ionization track to produce sputtering.

Based on results in Section 4 (see Figure 3), we see that, for relativistic grains with $\gamma > 1$, most ions have energy loss $dE/dx \leq 2 \times 10^{10} \text{ eV cm}^{-1}$, which is below the energy range where sputtering data are available. As result, the low-excitation energy regime is adopted for our calculations, which has the sputtering yield given by Equation (70) with $q = 3.3$. The sputtering for different ions is then calculated by the same formula but with their respective stopping power.

The sputtering yields by different atoms are shown in Figure 14 for silicate (left panels) and graphite (right panels) grains. We adopt $U = 5.7 \text{ eV}$ for silicate and $U = 4 \text{ eV}$ for graphite grains. We can see that the electronic sputtering is very sensitive to ions, which is determined by their energy loss in the grain. The sputtering from heavy ions Fe is the most important, which can reach $Y_{\text{sp}} \sim 10^{-2}$ atoms/ion for silicate. The sputtering by abundant, light elements (H, He) is negligible. Electronic sputtering for graphite is even less efficient.

7.3. Grain Destruction by Sputtering

Let X_i be the relative abundance of element i relative to hydrogen. The total sputtering yield is obtained by summing over all atomic elements in the ISM:

$$Y_{\text{sp}} = \sum_i X_i Y_{\text{sp},i}. \quad (71)$$

For calculations here, we assume that the elements throughout the ISM have solar abundance given in Draine (2011), although the abundance of elements in the ISM varies depending on the host galaxy.

When the total sputtering is known, the rate of destruction by sputtering for a grain of size a is equal to

$$\frac{dN_{\text{sp}}}{dt} = (n_{\text{gas}} \beta c) Y_{\text{sp}} \pi a^2. \quad (72)$$

The ejection of grain atoms corresponds to the decrease in the grain mass

$$\frac{dM_{\text{gr}}}{dt} = \rho 4\pi a^2 \frac{da}{dt}. \quad (73)$$

Using $dM_{\text{gr}}/dt = -\mu_T m_H dN_{\text{sp}}/dt$ with μ_T being the mean atomic weight of the dust, the rate of grain size decrease due to the sputtering is equal to

$$\frac{da}{dt} = -\left(\frac{n_{\text{gas}}}{4\rho}\right) \beta c \mu_T m_H Y_{\text{sp}}, \quad (74)$$

$$\approx -0.1 \hat{n}_{\text{gas}} \frac{\mu_T m_H}{m_C} \left(\frac{\beta}{0.1}\right) \left(\frac{Y_{\text{sp}}}{10^{-5}}\right) \mu\text{m Myr}^{-1}, \quad (75)$$

where $\hat{n}_{\text{gas}} = n_{\text{gas}}/10 \text{ cm}^{-3}$ and m_C carbon atomic mass.

Assuming the slowing down of dust grains is negligible and the same abundance in the Galaxy, we can estimate the total column gas density that the grain collides with before destruction by sputtering as follows:

$$N_{\text{coll}} = \frac{4\rho a}{Y_{\text{sp}} \mu_T m_H} \approx 6 \times 10^{23} \hat{\rho} a_{-5} \frac{m_C}{\mu_T m_H} \left(\frac{10^{-5}}{Y_{\text{sp}}}\right) \text{ cm}^{-2}, \quad (76)$$

From Figure 15, it can be seen that the sputtering rate rapidly declines from $\gamma = 1$ to the minimum at $\gamma \sim 2$ and starts to rise rapidly with increasing γ . The destruction time for $\gamma > 100$ is $\tau_{\text{sp}} = a/|da/dt| \sim 30 \times 10^4 (10^{-5}/Y_{\text{sp}}) a_{-5} \text{ Myr}$, and it takes longer time to destroy $\gamma < 100$ grains due to the decrease of the sputtering yield.

For silicate grains having $Y_{\text{sp}} \sim 10^{-5}$, we can see that relativistic silicate grains can be destroyed after sweeping a gas column density of $N_{\text{coll}} \sim 10^{24} a_{-5} \text{ cm}^{-2}$, while graphite grains would be destroyed after $N_{\text{coll}} \sim 10^{26} a_{-5} \text{ cm}^{-2}$ with $Y_{\text{sp}} \sim 10^{-6}$.

7.4. Destruction by Grain-Grain Collisions

For relativistic grains, grain-grain collision can be considered as the simultaneous bombardment of a target grain by a large number of neutral atoms from the projectile grain. The target grain is then rapidly heated to high temperature by photoelectrons produced during the collision. As a result, the evaporation of dust atoms from the grain surface becomes very efficiently.

Let a be the size of the projectile grain and a_T be the size of the target grain. The energy transferred from the projectile grain to target grain is equal to

$$\Delta E \sim \left(\frac{m_{\text{gr}}}{\mu_T m_H}\right) \times \frac{4a_T}{3} \frac{dE}{dx}. \quad (77)$$

The transient grain temperature can be estimated as $T_d = \Delta E/C_V$ with $C_V = 3n_d V k_B$ be the volume heat capacity for high-temperature limit and $n_d V = 10^{-14} a_{T,-5}^3 / (\mu_T m_H)$. Thus,

$$\begin{aligned} T_d &\sim \left(\frac{a}{a_T}\right)^3 \frac{4a_T}{9} \frac{dE/dx}{k_B} \\ &\sim 2.1 \times 10^7 \left(\frac{a}{a_T}\right)^3 a_{T,-5} \left(\frac{dE/dx}{4 \times 10^8 \text{ eV cm}^{-1}}\right) \end{aligned} \quad (78)$$

where the typical energy loss of a C atom with $\gamma < 100$ is $dE/dx = 4 \times 10^8 \text{ eV cm}^{-1}$ has been used for the numerical

estimate (see Figure 3), and projectile and target grains have similar n_d . Larger γ will result in an increased T_d .

The radiative cooling time of the grain at temperature T_d can be evaluated as the following:

$$\tau'_c = \frac{n_d (4\pi a_T^3/3) k_B T_d}{4\pi a_T^2 \sigma T_d^4}, \quad (79)$$

where each target atom is assumed to have thermal energy $k_B T_d$.

In order for the sublimation to be important, the sublimation time τ'_{sub} in the GF (Eq. 48 without γ) must satisfy the condition $\tau'_{\text{sub}} < \tau'_c$. Comparing these two timescales, one obtains $T_d > 3800 \text{ K}$ for silicate grains, which yields $a/a_T > a_c/a_T \sim 0.06$. This limit is apparently higher for graphite grains. Thus, we adopt the critical size of the projectile grain $a_c = 0.1 a_T$ for the complete destruction of the target refractory grain by a single collision.

The rate of hard-sphere collision between two grains of size a_T and a is given by

$$R_{\text{coll}}(a, a_T) = n(a) \beta c \pi (a^2 + a_T^2), \quad (80)$$

where $n(a) = dn/da$ is the density of dust grain of size a . The total collision rate that results in the complete evaporation of the target grain is obtained by integrating over the grain size distribution:

$$R_{\text{coll}} = \int_{a_c}^{a_{\text{max}}} R(a, a_T) \frac{dn}{da} da = \int_{a_c}^{a_{\text{max}}} \pi (a^2 + a_T^2) \beta c \frac{dn}{da} da, \quad (81)$$

where a_{max} is the upper cutoff of grain size distribution.

For the size distribution $dn = n_{\text{gas}} A_{\text{MRN}} a^{-3.5} da$ from Mathis et al. (1977) with $A_{\text{MRN}} = 10^{-25.16} \text{ cm}^{2.5}$, we obtain

$$\begin{aligned} R_{\text{coll}}(a_T) &= \pi n_{\text{gas}} A_{\text{MRN}} \beta c \\ &\times \left[\frac{a_T^2}{2.5} (a_c^{-2.5} - a_{\text{max}}^{-2.5}) - 2 (a_c^{-0.5} - a_{\text{max}}^{-0.5}) \right] \end{aligned} \quad (82)$$

For the ISM with $n_{\text{gas}} = 10 \text{ cm}^{-3}$, our estimates yield $R_{\text{coll}} = 7.9 \times 10^{-2} \text{ yr}^{-1}$ for $a_T = 0.1 \mu\text{m}$ and $R_{\text{coll}} = 2.2 \times 10^{-2} \text{ yr}^{-1}$ for $a_T = 1 \mu\text{m}$. Thus, the grain-grain collisions can destroy grains on a timescale of 1000 years.

Assuming that the gas-to-dust mass ratio is constant in the ISM, the gas column density that the relativistic grain has collided with between two successive collisions is equal to

$$\begin{aligned} N_{\text{coll}} &= R_{\text{coll}}^{-1} c \beta n_{\text{gas}} \\ &\approx \pi^{-1} A_{\text{MRN}}^{-1} \left[\frac{a_T^2}{2.5} (a_c^{-2.5} - a_{\text{max}}^{-2.5}) - 2 (a_c^{-0.5} - a_{\text{max}}^{-0.5}) \right]^{-1} \end{aligned} \quad (83)$$

Equation (83) yields $N_{\text{coll}} \approx 10^{20} \text{ cm}^{-2}$ and $4 \times 10^{20} \text{ cm}^{-2}$ for $a_T = 0.1 \mu\text{m}$ and $1 \mu\text{m}$, respectively.

8. DISCUSSION

It has been more than 60 years since the original idea of relativistic dust was introduced as a source of heavy cosmic-ray particles by Spitzer (1949) and was suggested as primary particles of UHECRs by Hayakawa (1972a), a number of theoretical studies and observational measurements have been done. Nevertheless, the question whether relativistic dust can reach our solar system as

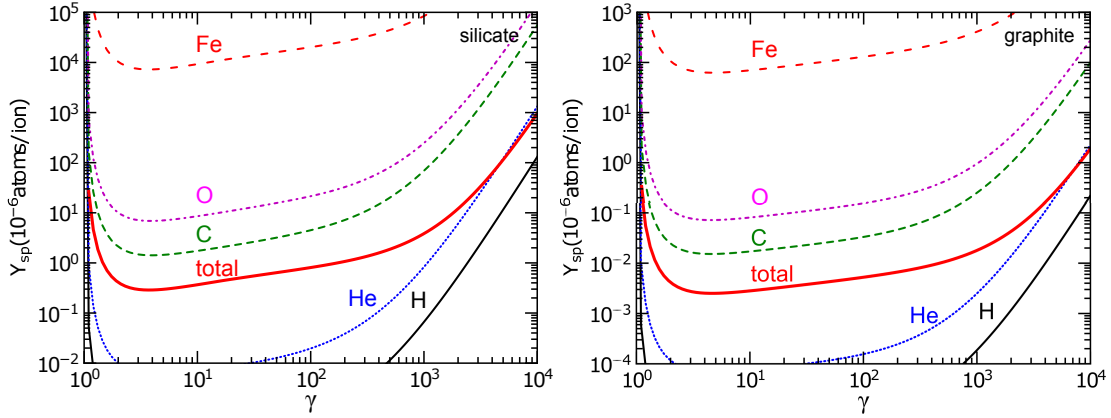


FIG. 14.— Electronic sputtering yield Y_{sp} vs. γ for silicate (left) and graphite grains (right) bombarded by H, He, C, O and Fe atoms. The yield is significant for Fe but negligible for H and He.

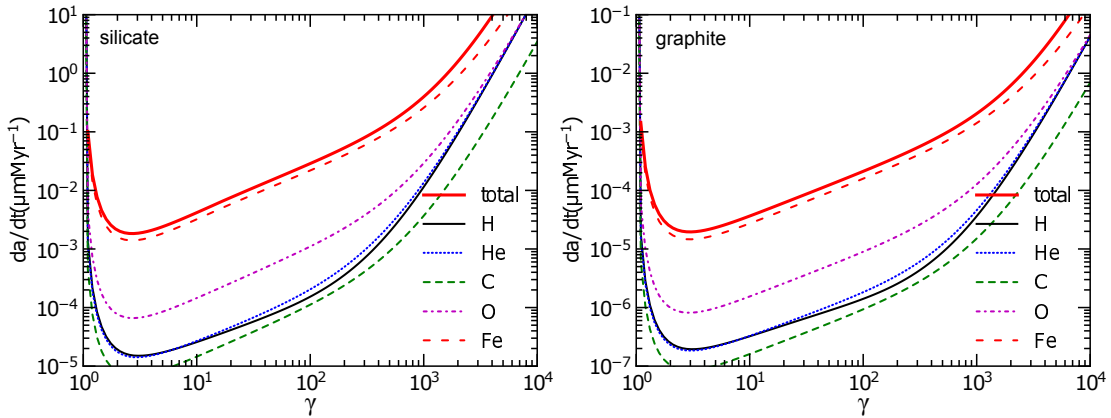


FIG. 15.— Sputtering rate $|da/dt|$ vs. γ for silicate (left) and graphite grains (right) bombarded by several atoms. The total sputtering rate is shown in solid lines. The minimal sputtering rate at $\gamma \sim 2$ corresponds to the minimum ionization cross-section by electronic interactions in the high-energy regime.

UHECRs still remains. With significant advance in physics of solid state and astrophysics dust during the last decades, it is now time for us to reexamine this interesting idea and to seek for a better understanding on origin and destruction of relativistic dust and its implications for UHECRs.

8.1. Grain destruction in the interstellar medium

Before entering the solar system, relativistic grains travel through the ISM, and the interactions of the grain with ambient gas and dust are certainly important for grain destruction. The collisional destruction due to electronic sputtering by ions and grain-grain collisions is studied in detail in Section 7.

For electronic sputtering, we found that heavy Fe ions are the most important, which can produce a considerable yield $Y_{\text{sp}} \sim 10^{-2}$, whereas lighter ions (e.g., H, He, C) induce negligible yields. When the solar abundance of elements is assumed, the net sputtering yield turns out to be $Y_{\text{sp}} \sim 10^{-5}$ and 10^{-6} for silicate and graphite grains, respectively. Therefore, electronic sputtering only destroys the grain after it sweeps with a huge column density of gas $N_{\text{coll}} \sim 10^{24} a_{-5} \text{ cm}^{-2}$ for silicate and $N_{\text{coll}} \sim 10^{26} a_{-5} \text{ cm}^{-2}$ for graphite grains.

The destruction by grain-grain collisions is estimated to be the most efficient. We find that a single grain-grain collision can impulsively heat the target grain to above the sublimation temperature due to the transfer

of photoelectrons to the entire grain. As a result, the evaporation followed by the single grain-grain collision can completely destroy the grains. The size of the projectile grain is about 10 percent of the target size for the evaporation to be significant. Using the MRN grain size distribution, we found that grain-grain collisions can destroy relativistic grains after sweeping a gas column density $N_{\text{coll}} \leq 4 \times 10^{20} \text{ cm}^{-2}$ for $a \leq 1 \mu\text{m}$.

Now, let us consider grain heating and charging by the interstellar radiation field (ISRF), which has energy spectrum $u(\nu)$ estimated in the solar neighborhood from Mathis et al. (1983). Assuming that the ISRF is isotropic, the density of radiation energy in the GF is related to $u(\nu)$ through Equation (B4). The collisional heating by the ambient gas is also taken into account through Equation (41).

Figure 16 shows the obtained equilibrium temperature for silicate and graphite grains. At $\gamma = 1$, grains at rest in the plasma, the grain temperature is determined by radiative heating from interstellar photons. When γ is slightly above 1, collisional heating becomes important, which results in a jump in T_d . It can be seen that, for different grains, T_d is much lower than the melting/sublimation limit. Thus, relativistic grains could easily survive heating in the ISM.

To quantify the effect of Coulomb explosions for relativistic grains moving in the ISM, we estimate the distance that the grain has traveled before exploding by

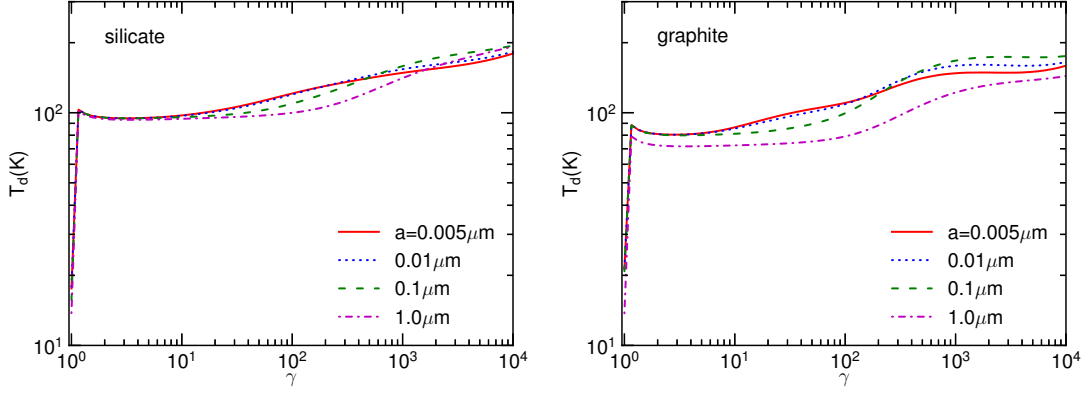


FIG. 16.— Grain equilibrium temperature T_d vs. γ for silicate (left) and graphite (right) grains heated by the ISRF and ion collisions. Different grain sizes a are considered. $T_d < 21$ K for stationary grains with $\gamma = 0$ and quickly rises when γ slightly above unity due to the contribution of collisional heating by gaseous species. A jump of T_d at $\gamma \sim 1$ is caused by collisional heating of ambient gas. T_d increases slowly with increasing γ for $\gamma > 1$.

integrating Equation (58) from $Z = 0$ to $Z = Z_{\max}$:

$$L_{\max} = \gamma \beta c \int_0^{Z_{\max}} \frac{dZ}{J_{\text{tot}}(a, Z)}. \quad (84)$$

Figure 17 shows the resulting L_{\max} as a function of γ for different grain sizes. It indicates that big grains of $\gamma < 10^3$ are more likely to survive, but small ($a \leq 0.01 \mu\text{m}$) grains are quickly destroyed by Coulomb explosions when moving with $\gamma > 5$.

8.2. Grain destruction in the intergalactic medium

The IGM is fully ionized plasma and filled with CMB photons. Using the sputtering rate calculated for the ISM (Eq. 74), one can obtain

$$\left(\frac{da}{dt}\right) \approx 1.6 \times 10^{-6} \frac{n_{\text{IGM}}}{10^{-4} \text{ cm}^{-3}} \frac{m_C}{m_T} \left(\frac{\beta}{0.1}\right) \left(\frac{10^{-5}}{Y_{\text{sp}}}\right) \mu\text{m Myr}^{-1}$$

where n_{IGM} is the number density of the IGM.

For the typical IGM density $n_{\text{IGM}} = 10^{-4} \text{ cm}^{-3}$, it would take $t_{\text{sp}} \approx 60 a_{-5}$ Gyr to destroy the relativistic grains of $\beta \sim 1$ via sputtering. Thus, the sputtering of relativistic dust is negligible in the IGM. The presence of intergalactic dust certainly disfavors the survival of relativistic dust since a single grain-grain collision can destroy the grain completely.

The destruction by CMB photons is also expected to be unimportant. Indeed, the averaged energy of CMB photon is $h\nu_{\text{CMB}} = 2.7 k_B T_{\text{CMB}} \approx 6.34 \times 10^{-4} \text{ eV}$. In the GF, the CMB photon energy is boosted to $h\nu' = \gamma h\nu_{\text{CMB}} = 6.34 \times 10^{-4} \gamma \text{ eV}$. Due to its lower energy, the CMB photons cannot heat the grains above the melting temperature.

In order for CMB photons to ionize grains, the photon energy must be boosted to $h\nu' > W$, which requires $\gamma > 10^4$. The value γ needed for Coulomb explosions must be much higher since $\text{IP}(Z_{\max}) \gg W$. Thus, relativistic grains are freely moving through the IGM until they encounter an intergalactic grain and may be completely evaporated.

8.3. Grain destruction in the solar radiation field and UHECRs

Solar radiation field is the most important and final barrier that relativistic grains must overcome to become primary particles of UHECRs.

Our detailed calculations show that melting and sublimation play an important role for relativistic grains in this radiation field. For instance, silicate grains are found to melt at distance $R_m < 10$ AU from the Sun while larger grains or higher γ have larger R_m . Graphite grains melt at much smaller distance (i.e., $R_m \sim 2$ AU) when a high melting temperature $T_m = 4000$ K is taken.

The remaining question is whether grains will be destroyed after melting. The answer is uncertain. Nevertheless, if after melting, a big liquid grain (drop) somehow is transformed into a number of droplets, then these droplets seem to be easily destroyed by Coulomb explosions than the primary drop due to their lower maximum electrostatic potential ϕ_{\max} (see Section 6).⁸

Moreover, when the grain temperature T_d exceeds the melting point, the sublimation becomes important. While approaching the Sun from $R_m > 1$ AU, T_d continues to rise rapidly due to the increase of radiation flux, which is accompanied with the rapid evaporation of atoms from the grain surface. As a result, to distance of 1 AU, the sublimation can substantially decrease the grain size, resulting in the complete destruction of some relativistic grains.

Figure 18 summarizes the parameter space (a, γ) that the silicate and graphite grains would be destroyed by and survive Coulomb explosions and sublimation in the solar radiation field. It appears that Coulomb explosions are an important destruction mechanism for both silicate and graphite grains, and sublimation is dominant mostly for silicate grains.

The grains with (a, γ) located in the gray areas in Figure 18 would survive both Coulomb explosions and sublimation and reach the Earth as primary particles of UHECRs. After entering the Earth atmosphere, the relativistic grain would produce a huge extensive air shower corresponding to the superposition of 10^{10} shower events. The depth of maximum shower is expected to be high in the Earth atmosphere. Measurements for the depth of maximum showers show that the data are well con-

⁸ The paper has assumed dust grains of compact structure. For porous grains with inclusions of gas molecules within the grain's cavity, the pore gas will likely melt at lower temperatures (i.e., higher solar distances). As a result, the Coulomb repulsion between different surface areas on a non-spherical grain may help to break a liquid solid into multiple droplets after melting.

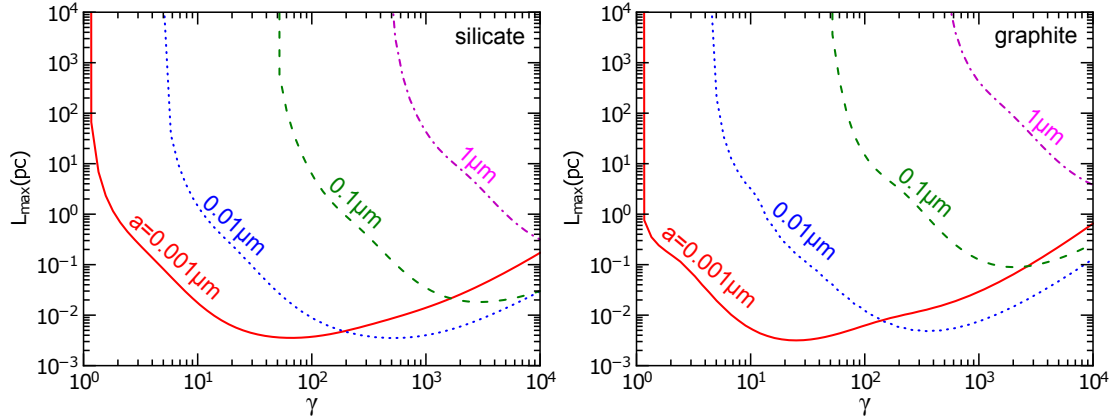


FIG. 17.— Maximum distance L_{\max} vs. γ for silicate (left) and graphite (right) grains. Very small grains ($a \sim 0.001 \mu\text{m}$) are rapidly destroyed, and big grains ($a \sim 1 \mu\text{m}$) can travel a huge distance if $\gamma < 10^3$.

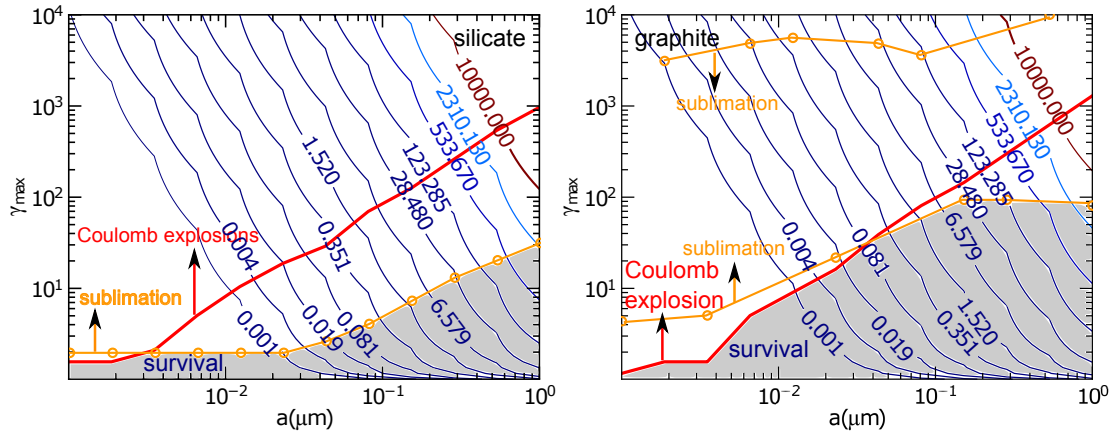


FIG. 18.— Maximum Lorentz factor γ_{\max} for grain survival against Coulomb explosions (thick solid line) and sublimation (solid line with circle symbols) vs. grain size a for silicate (left) and graphite (right). Contours show $E_{\text{gr}}(a, \gamma_{\max})$ levels in units of 10^{20} eV. Grains with (a, γ) located above the red line (gold line) are destroyed by Coulomb explosions (sublimation) and those with (a, γ) located below these lines will survive. Gray areas show the grains that survive both Coulomb explosions and sublimation.

strained by theoretical predictions with the upper bound produced by primary protons and lower bound by heavy atomic nuclei (see e.g., Aloisio et al. 2012).

The grains with (a, γ) located above the solid lines (with circle symbols) would be destroyed by sublimation while gradually releasing heavy nuclei from the melting distance $R_m < 10$ AU. Scattering of solar photons by the ejected nuclei is expected to produce gamma-rays, as originally suggested by Grindlay & Fazio (1974). The grains with (a, γ) above the thick solid lines would explode within distance less than 10^5 AU from the Sun, simultaneously releasing a huge number of relativistic heavy nuclei. Such relativistic nuclei may create gamma-ray bursts due to scattering of solar photons.

8.4. Can dust grains be accelerated to relativistic speeds?

Our theoretical calculations indicate that there exist some range of (a, γ) that relativistic grains could reach the Earth atmosphere and contribute to the $E > 10^{20}$ eV primary particles of UHECRs. The question now is what physical processes potentially accelerate grains to relativistic speeds.

First, radiation pressure by powerful radiation sources, such as quasars and Seyfert galaxies, is found to be able to accelerate silicate grains to maximum speeds of $\gamma < 5$ for grains initially located within a distance of

several sublimation radius r_{sub} from the central source. However, the extragalactic relativistic dust can be efficiently destroyed by grain-grain collisions and has little chance to reach our Galaxy. Meanwhile, radiation pressure from supernovae in the Galaxy can accelerate grains to $v \sim 0.1c$ speeds. These subrelativistic grains may reach the Earth but require further acceleration to become important for UHECRs.

Second, diffusive shocks of SNRs, which are widely believed to be important for the acceleration of CRs (Blandford et al. 1978), are also found to be important for charged grains by theoretical study (Ellison et al. 1997) and numerical simulations (Giacalone et al. 2009). However, assuming a high shock speed $V_{\text{sh}} = 10^4 \text{ km s}^{-1}$, the maximum grain velocity achieved by diffusive shocks is about several tenths of the light speed for a typical interstellar magnetic field $B \sim 10 \mu\text{G}$. Since the magnetic field may be amplified in the shock by streaming instability (Berezhko et al. 2003; Beresnyak et al. 2009; Riquelme & Spitkovsky 2010), we expect the grain velocity acquired from shock acceleration would be significantly enhanced.

Third, charged grains can be accelerated by resonance acceleration (Lazarian & Yan 2002; Yan et al. 2004) and transit time damping (Hoang et al. 2012) by fast modes of magnetohydrodynamic (MHD) turbulence. Very small

dust grains (e.g., polycyclic aromatic hydrocarbons) can be accelerated to a few times thermal velocity by charge fluctuations (Ivlev et al. 2010; Hoang & Lazarian 2012). Although the aforementioned acceleration mechanisms are only able to accelerate grains to subrelativistic speeds, they can provide sufficient injection energy for grains to enter diffusive shocks and to be accelerated to higher speeds.

Fourth, the acceleration of charged grains may also happen due to magnetic reconnection that gets fast in turbulent environments (Lazarian & Vishniac 1999; Kowal et al. 2009; Eyink et al. 2011, see Lazarian et al. 2014 for a review). The corresponding first-order Fermi mechanism suggested for cosmic rays (de Gouveia Dal Pino & Lazarian 2005; Lazarian 2005) has been successfully tested numerically (Kowal et al. 2012) and was invoked for explaining several space physics and astrophysical problems (see Lazarian & Opher 2009; Lazarian & Desiati 2010). We are confident that a similar mechanism should be efficient for the acceleration of charged grains. We shall provide more details of the acceleration of charged dust in reconnection sites in our subsequent paper.

Finally, relativistic shocks in extragalactic sources (e.g. AGN jets, gamma-ray bursts) may also be a potential source for relativistic grains. Nevertheless, as aforementioned, the extragalactic origin of relativistic grains as UHECRs would be limited due to efficient destruction by grain-grain collisions in the ISM of host galaxies as well as our Galaxy.

8.5. Effects of magnetic fields on acceleration and propagation of relativistic dust

A final issue related to the effect of ambient magnetic fields on the propagation of relativistic charged grains in the ISM. The ratio of magnetic pressure $p_{\text{mag}} = B^2/8\pi$ to radiation pressure is given by

$$\frac{p_{\text{mag}}}{p_{\text{rad}}} = \left(\frac{B^2}{8\pi}\right) \frac{4\pi r^2 c}{\langle Q_{\text{pr}}(a, \lambda) \rangle L}, \quad (86)$$

$$= 3.73 \times 10^{-10} B_{10}^2 r_{\text{pc}}^2 \left(\frac{10^{13} L_{\odot}}{L \langle Q_{\text{pr}} \rangle} \right) \quad (87)$$

where B is the magnetic field strength and $B_{10} = B/10\mu\text{G}$.

It can be seen that magnetic pressure is negligible compared to radiation pressure during the acceleration stage ($t \leq \tau_{\text{acc}}$) but is important when the grain moves through the ISM.

The grain motion in the ISM is inevitably constrained by the Lorentz force if it does not move along the mean magnetic field lines. The gyroradius of a charged grain moving across \mathbf{B} is equal to:

$$r_g = \frac{m_{\text{gr}} c v_{\perp}}{\langle Z \rangle e B}, \quad (88)$$

where $\langle Z \rangle e$ is the equilibrium charge of the grain.

For $v_{\perp} \sim c$, we get $r_g \sim 0.6 \langle Z \rangle^{-1} B_{10}^{-1} \hat{\rho} a_{-5}^3 \text{ kpc}$, which indicates that relativistic grains are confined within the host galaxy and unable to reach the Galaxy.

One should not assume that charged grains move along the field lines. However, due to magnetic field

wandering of Alfvénic component of MHD turbulence⁹ the grain will move perpendicular to the mean magnetic field, while following the local magnetic field direction. The corresponding field wandering is described in Lazarian & Vishniac (1999) and it results in superdiffusive behavior at scales less than the turbulence injection scale (see Lazarian & Yan 2014) and diffusive at scales less than the turbulence injection scale. The latter scale in our galaxy is associated with supernovae explosions and is around 100 pc. According to Equation (88) the superdiffusive behavior is going to be important only for grains with $a < 0.3 \mu\text{m}$.

9. SUMMARY

We revisited the idea of relativistic grains as primary particles of UHECRs by studying in detail various destruction mechanisms, including melting/sublimation and Coulomb explosions, electronic sputtering, and grain-grain collisions. Our principal results are summarized as follows:

1. The equilibrium temperature of relativistic grains heated by the solar radiation field and gaseous collisions is exactly calculated, accounting for the fraction of photon energy carried away by photoelectrons. We found that sublimation is a leading mechanism for the destruction of relativistic grains in the solar radiation field. The $0.1 \mu\text{m}$ silicate grains with Lorentz factor $\gamma > 5$ would be completely destroyed while graphite grains of comparable size are destroyed for $\gamma > 100$.
2. The photoelectric yield due to the emission of primary, Auger and secondary electrons is computed for dust grains moving with arbitrary γ . The total charging rate is used to compute the closest distance that relativistic grains can reach the Earth atmosphere before Coulomb explosions.
3. We found that Coulomb explosions can be a dominant mechanism for the destruction of relativistic grains with $\gamma > 10^2 - 10^3$, but grains with smaller γ can survive. Larger grains tend to be destroyed by Coulomb explosions starting from a higher γ due to their higher photoelectric threshold.
4. A survival window of parameters (a, γ) that relativistic grains could survive heating and Coulomb explosions in the solar radiation field is identified.
5. Relativistic grains can survive radiative heating by the interstellar radiation field and CMB, but the grains moving with $\gamma > 10^4$ will likely be destroyed by Coulomb explosions.
6. We study electronic sputtering by ions and its effect on the destruction of relativistic dust. Although heavy Fe ion is found to produce considerable sputtering yield ($Y_{\text{sp}} \sim 10^{-3} - 10^{-1}$), its low abundance makes the net sputtering yield rather small. The destruction by electronic sputtering is inefficient for relativistic grains.

⁹ A discussion and practical procedures of decomposing magnetic fields into Alfvénic, slow and fast modes are given in Cho & Lazarian (2002, 2003) and Kowal & Lazarian (2010).

7. The evaporation induced by grain-grain collisions is the most efficient destruction mechanism in the ISM, for which relativistic grains with $a \leq 1 \mu\text{m}$ can be completely destroyed after sweeping a gas column density $N_{\text{coll}} \leq 4 \times 10^{20} \text{cm}^{-2}$.
8. The extragalactic origin of relativistic dust appears to be limited due to the efficient destruction by grain-grain collisions in the local ISM of the host galaxy as well as magnetic confinement. Some grains accelerated to relativistic speeds by acceleration processes in the Galaxy might survive both the ISM and Solar radiation field to become pri-

mary particles of UHECRs.

We thank the referee for her/his insightful comments that significantly improved our paper. T.H. thanks Dr. Anthony Jones for useful discussion and comments on our paper. T.H. is supported by the Alexander von Humboldt Fellowship at the Ruhr-Universität Bochum. A.L. acknowledges the financial support of NASA grant NNX11AD32G and the Center for Magnetic Self-Organization and thanks IIP/UFRN (Natal) for hospitality. R.S. acknowledges partial support by the Deutsche Forschungsgemeinschaft grant Schl 201/29-1 and the Mercator Research Center Ruhr (MERCUR) grant Pr-2012-0008.

APPENDIX

A. DUST SURVIVAL RADIUS NEAR A POINT SOURCE OF RADIATION

The equilibrium temperature of dust at distance r heated by a central radiation source can be approximated by

$$T_d(r) = 1800 \left[\left(\frac{L_{\text{UV}}}{5 \times 10^{12} L_{\odot}} \right)^{1/2} \left(\frac{1 \text{ pc}}{r} \right)^2 \right]^{1/5.6} \text{ K}, \quad (\text{A1})$$

where L_{UV} is the luminosity in the optical and UV, which is about a half of the bolometric luminosity (see e.g., [Scoville & Norman \(1995\)](#)).

By setting T_d equal to the dust sublimation temperature T_{sub} , we obtain the closest distance that dust can survive as the following:

$$r_{\text{sub}} = \left(\frac{L_{\text{UV}}}{5 \times 10^{12} L_{\odot}} \right)^{1/2} \left(\frac{T_{\text{sub}}}{1800 \text{ K}} \right)^{-5.6/2} \text{ pc}. \quad (\text{A2})$$

For SN explosions with $L_{\text{UV}} \sim 5 \times 10^8 L_{\odot}$, we get $r_{\text{sub}} \sim 0.01 \text{ pc}$. For AGN with $L_{\text{UV}} \sim 10^{13} L_{\odot}$, we get $r_{\text{sub}} \sim 1 \text{ pc}$.

Due to radiation pressure, grains are rapidly accelerated to high velocities from r_{sub} . Comparing τ_{acc} with τ_{sub} , we see that grains initially at $r_i = r_{\text{sub}}$ are likely destroyed by sublimation before achieving their terminal velocities, while grains with $r_i \geq 1.5 r_{\text{sub}}$ will survive the sublimation and get their highest velocities.

The interstellar medium surrounding AGNs is fully ionized by its strong UV radiation. The grain equilibrium charge due to photoelectric emission and collisional charging is estimated by

$$\langle Z \rangle = 1.3 \times 10^3 a_{-5} \left(\frac{L_{\gamma 13}}{n_{e8} r_{\text{pc}}^2} \right)^{2/11} T_{e4}^{1/11}, \quad (\text{A3})$$

where L_{γ} is the total UV and X-ray luminosity and $L_{\gamma 13} = L_{\gamma}/10^{13} L_{\odot}$, $n_{e8} = n_e/10^8 \text{cm}^{-3}$ is the electron number density, and $T_{e4} = T_e/10^4 \text{ K}$ is the gas temperature (see more details in [Scoville & Norman 1995](#)).

For diffuse medium which is important for grain acceleration $n_e < 10^4 \text{cm}^{-3}$, $\langle Z \rangle < 10^4 a_{-5} \left(\frac{L_{\gamma 13}}{n_{e4} r_{\text{pc}}^2} \right)^{2/11} T_{e4}^{1/11}$. Comparing to Z_{max} , we can see that the $a > 0.01 \mu\text{m}$ grains would be unlikely destroyed by Coulomb explosions.

At distance $r \sim 100 \text{ pc}$ from quasars with $L_{\gamma} \sim 10^{13} L_{\odot}$ where grains have achieved terminal velocity, we get $\langle Z \rangle = 4285 a_{-5}$ for the ISM with $n_e = 10 \text{cm}^{-3}$ and $T_e \sim 5000 \text{ K}$.

B. TRANSFORMATIONS OF RADIATION FIELDS BETWEEN STATIONARY FRAME AND COMOVING GRAIN'S REFERENCE FRAME

Assuming that a dust grain is moving with $\gamma \gg 1$ in a radiation field. Let $\mu = \cos \theta$ be the cosine angle between the direction of grain motion and that of photon propagation, and let $u(\nu, \Omega) = dE/d\nu d\Omega dV$ be the specific spectral energy density of radiation in the SF. In the GF, the photon energy $h\nu'$ and specific spectral energy density $u'(\nu', \Omega')$ are governed by the following transformations:

$$\frac{u(\nu, \Omega)}{\nu^3} = \frac{u'(\nu', \Omega')}{\nu'^3}, \quad \frac{n(\nu, \Omega)}{\nu^2} = \frac{n'(\nu', \Omega')}{\nu'^2}, \quad \nu' = \gamma\nu(1 - \beta\mu), \quad \mu' = \frac{\mu - \beta}{1 - \beta\mu}, \quad d\mu' = \frac{d\mu}{\gamma^2(1 - \beta\mu)^2} = \frac{d\mu}{\mathcal{D}^2}, \quad (\text{B1})$$

where $n = u/\nu$ and $n' = u'/\nu'$ are the photon density in the SF and GF, respectively (see [Dermer & Schlickeiser 2002](#)).

The spectral energy density is given by

$$u(\nu) = \int d\Omega u(\nu, \Omega). \quad (\text{B2})$$

For an *isotropic* radiation field, $u(\nu, \Omega) = u(\nu)/4\pi$, and we obtain

$$u'(\nu', \Omega') = \frac{u(\nu)}{4\pi} \mathcal{D}^3, \text{ or } u'(\nu', \mu') = \frac{u(\nu)}{2} \mathcal{D}^3, \quad (\text{B3})$$

where $\mathcal{D} = \gamma(1 - \beta\mu)$ is the Doppler parameter, and the symmetry of emission over the azimuthal angle is assumed.

The energy density of radiation from an isotropic source in the GF is then equal to

$$\begin{aligned} u'(\nu') d\nu' &= \int d\mu' u(\nu', \mu') d\nu' = d\nu' \int_{-1}^1 \frac{d\mu}{\mathcal{D}^2} \frac{u(\nu)}{2} \mathcal{D}^3 = d\nu' \frac{u(\nu)}{2} \int_{-1}^1 d\mu \mathcal{D}^2, \\ &= u(\nu) d\nu \times \frac{1}{2} \int_{-1}^1 d\mu \gamma^2 (1 - \beta\mu)^2 = u(\nu) d\nu \gamma^2 \left(1 + \frac{\beta^2}{3}\right), \end{aligned} \quad (\text{B4})$$

where the integration over μ is taken from -1 to 1 , over the entire space of isotropic incident radiation. Cosmic microwave background (CMB) radiation and interstellar radiation field (ISRF) are examples for the isotropic radiation field.

The total energy density from the isotropic radiation field in the GF is then equal to

$$u'_{\text{rad}} = \int d\nu' u'(\nu') = \int d\nu u(\nu) \gamma^2 \left(1 + \frac{\beta^2}{3}\right) = u_{\text{rad}} \gamma^2 \left(1 + \frac{\beta^2}{3}\right), \quad (\text{B5})$$

where $u_{\text{rad}} = \int d\nu u(\nu)$.

For a *unidirectional* radiation field from a point source (e.g., Sun) with luminosity $L = \int L_\nu d\nu$,¹⁰ the specific spectral energy density $u(\nu, \mu)$ can be represented through a δ function as follows:

$$u(\nu, \mu) = \frac{L_\nu}{4\pi d^2 c} \delta(\mu - \mu_{\text{gr}}), \quad (\text{B6})$$

where $f = L_\nu/4\pi d^2$ is the flux of radiation energy at the grain's position, and $\delta(\mu - \mu_{\text{gr}})$ denotes the fact that the flux of radiation energy is defined as the energy propagating through an surface unit perpendicular to the the radiation direction (i.e., $\mu_{\text{gr}} = \pm 1$). The spectral energy density from a point source is given by the usual expression:

$$u(\nu) = \int d\mu u(\nu, \mu) = \frac{L_\nu}{4\pi d^2 c}. \quad (\text{B7})$$

In the GF, the incident radiation becomes focused, and we obtain $u(\nu') d\nu' = \int d\mu' u(\nu', \mu') d\nu'$ as the following:

$$\begin{aligned} u'(\nu') d\nu' &= \int d\mu' u(\nu, \mu) \mathcal{D}^3 (\mathcal{D} d\nu) = \int d\mu' \mathcal{D}^4 \frac{L_\nu}{4\pi d^2 c} \delta(\mu - \mu_{\text{gr}}) d\nu = \frac{L_\nu}{4\pi d^2 c} d\nu \int_{-1}^1 \frac{d\mu}{\mathcal{D}^2} \delta(\mu - \mu_{\text{gr}}) \mathcal{D}^4, \\ &= \frac{L_\nu}{4\pi d^2 c} d\nu \int_{-1}^1 d\mu \delta(\mu - \mu_{\text{gr}}) \gamma^2 (1 - \beta\mu)^2 = u(\nu) d\nu \int_{-1}^1 d\mu \gamma^2 (1 - \beta\mu)^2 \delta(\mu - \mu_{\text{gr}}), \\ &= u(\nu) d\nu \gamma^2 (1 - \beta\mu_{\text{gr}})^2. \end{aligned} \quad (\text{B8})$$

where $\mu_{\text{gr}} = -1$ for the case the grain arrives from the direction opposite to the Sun.

The total energy density from a point source in the GF is then equal to

$$u'_{\text{rad}} = \int d\nu' u'(\nu') = \int d\nu u(\nu) \gamma^2 (1 - \beta\mu_{\text{gr}})^2 = u_{\text{rad}} \gamma^2 (1 - \beta\mu_{\text{gr}})^2. \quad (\text{B9})$$

In the assumption of monochromatic approximation, the spectral energy density of radiation can be represented through u_{rad} by a δ function:

$$u(\nu) = u_{\text{rad}} \delta(\nu - \bar{\nu}). \quad (\text{B10})$$

where $h\bar{\nu}$ is the average energy of a photon, and u_{rad} (erg cm^{-3}) is the total energy density.

C. PHOTOEMISSION OF ELECTRONS FROM DUST BY X-RAY

In the GF, optical or near-UV photons appear as X-ray. The interactions of photons with relativistic dust grains is similar to those of X-ray photons with stationary grains. For completeness, below, we summarize earlier works on the photoemission of electrons from stationary dust grains by X-ray.

¹⁰ The spectral luminosity from a star of radius R_\star and surface

temperature T_\star is $L_\nu = 4\pi R_\star^2 \pi B_\nu(T_\star)$ where $B_\nu(T_\star)$ is the Planck function, and $L = \int L_\nu d\nu = 4\pi R_\star^2 \sigma T_\star^4$.

C1. Ionization Potential and Photoelectric Yield

The energy threshold for photoemission is given by

$$h\nu_{\text{pet}} = \text{IP}(Z) \text{ for } Z \geq -1, \text{ and } h\nu_{\text{pet}} = \text{IP}(Z) + E_{\text{min}} \text{ for } Z < -1. \quad (\text{C1})$$

where $\text{IP}(Z)$ is the ionization potential for valence band of a grain of charge Z , which is given by

$$\text{IP}(Z) = W + \left(Z + \frac{1}{2}\right) \frac{e^2}{a} + (Z + 2) \frac{e^2}{a} \frac{0.3\text{\AA}}{a} \quad (\text{C2})$$

and

$$E_{\text{min}} = 0 \text{ for } Z \geq -1, \quad (\text{C3})$$

$$E_{\text{min}} = \theta(\nu = |Z + 1|) \left(1 - 0.3 \left(\frac{a}{10\text{\AA}}\right)^{-0.45} |Z + 1|^{-0.26}\right) \text{ for } Z < -1. \quad (\text{C4})$$

where θ is given in [Draine & Sutin \(1987\)](#).

TABLE 1
ATOMIC STRUCTURE AND IONIZATION POTENTIAL (eV)

Atoms	K	L1	L2	L3	M1	M2	M3	M4
C	291.01	17.56
O	537.28	29.23
Mg	1294.50	89.46	56.55	56.24	6.89
Si	1828.50	151.55	108.67	107.98	13.63
Fe	7083.40	842.96	733.55	720.69	101.01	68.04	66.45	12.91

Ionization potential for inner electronic shells is listed in Table 1.

The photoelectric yield is determined by as the following:

$$Y(h\nu, Z, a) = y_2(h\nu, Z, a) \min[y_0(\Theta)y_1(a, h\nu), 1], \quad (\text{C5})$$

where $y_0(\Theta)$ with $\Theta = h\nu - \text{IP}(Z)$ describes the fact that photon energy must be higher than ionization potential to ionize grains, $y_1(a, h\nu)$ describes the fact that a photoelectron produced inside the grain must not be absorbed by dust material to reach the surface, and $y_2(h\nu, aZ)$ describes the fact that the photoelectron must overcome the potential barrier of valence band to escape from the grain surface to infinity. Detailed expressions for y_0 , y_1 and y_2 are presented in [Weingartner et al. \(2006\)](#).

The absorption cross-section $\sigma_{i,s}$ for shell s of element i is taken from [Verner et al. \(1996\)](#), using the FORTRAN code phfit2 via the link <http://www.pa.uky.edu/~verner/fortran.html>.

C2. Charging by Compton Scattering

For very high-energy photons with $E > 10^4$ eV, which is much larger than the binding energy of the K-shell electrons, the interaction of photons with atoms of a dust grain can be considered as the interaction with free electrons. During scattering, electron energy is boosted due to the transfer of photon energy to the electron via Compton effect. Some scattered electrons will escape from the grain if their energy is above the potential barrier and becomes the free electrons, producing positively charged grains.

The maximum energy of an electron obtained from Compton scattering is given by

$$\epsilon_e(\gamma) = h\nu' \frac{\alpha(1 - \cos\theta)}{1 + \alpha(1 - \cos\theta)} = \gamma h\nu \frac{2\alpha}{1 + 2\alpha}, \quad (\text{C6})$$

where $\alpha = h\nu'/m_e c^2 = \gamma h\nu/m_e c^2$ and the head-on collision ($\theta = 180^\circ$) is assumed.

To estimate the critical energy that electrons need to escape from the grain, ϵ_{cr} , we note that the energy loss within the dust grain can be described by an empirical law for nonrelativistic electrons ([Bingham et al. 1999](#)):

$$\frac{d\epsilon_e}{dl} \approx 10^{-6} \frac{\rho m_e c^2}{\epsilon_e}. \quad (\text{C7})$$

In order for a scattered electron with energy ϵ_e to escape from the grain surface, the range of electron must be $R_e(E) \sim \epsilon_e/(d\epsilon_e/dl) \geq a$, which corresponds to

$$\frac{d\epsilon_e}{dl} \geq \frac{\epsilon_e}{a}. \quad (\text{C8})$$

From Equations (C7) and (C8) we obtain

$$\epsilon_e \geq \epsilon_{cr1} \equiv m_e c^2 (a\rho)^{1/2} = 2.8 \times 10^3 a_{-5}^{1/2} \hat{\rho}^{1/2} \text{ eV}, \quad (\text{C9})$$

where $m_e c^2 \approx 10^{-6} \text{ erg}$ has been used.

For a grain with nonzero charge, the electron energy must be higher than the grain's Coulomb potential to leave the surface:

$$\epsilon_e \geq \epsilon_{cr,2} \equiv \frac{Ze^2}{a} = 0.014 Z a_{-5}^{-1} \text{ eV}. \quad (\text{C10})$$

Using $Z = Z_{\text{max}}$ for the above equation, we obtain

$$\epsilon_{cr2} = 1.06 \times 10^3 \left(\frac{S_{\text{max}}}{10^{10} \text{ dyn cm}^{-2}} \right)^{1/2} a_{-5} \text{ eV}. \quad (\text{C11})$$

From Equations (C10) and (C6), we see that photons must have energy $\gamma h\nu \geq 10^5 \text{ eV}$ to produce free electrons via the inverse Compton scattering. For solar photons with the averaged energy $h\nu_\odot = 1.34 \text{ eV}$, the charging by Compton scattering is important for $\gamma > 10^5$. Nevertheless, the Compton effect can be important for lower γ thanks to photons emitted in the blue part of the radiation spectrum.

Bingham et al. (1999) considered the Compton scattering by photons in the Wein part of thermal spectra and obtained the charging rate at distance R from the Sun as the following:

$$J_C = \left(\frac{\text{AU}}{R} \right)^2 \left(\frac{7\pi\gamma\sigma_T c a^3}{m_H} \right) \left(\frac{k_B T_\odot}{\hbar c} \right)^3 \exp \left[-\frac{m_e c^2}{2\gamma k_B T_\odot} \left(\frac{\epsilon_{cr}}{2m_e c^2} \right)^{1/2} \right], \quad (\text{C12})$$

where σ_T is the Thompson scattering cross-section, $\epsilon_{cr} = \max[\epsilon_{cr1}, \epsilon_{cr2}]$ is the critical kinetic energy for which electron can escape the grain surface to become free electron.

Since $\epsilon_{cr1} > \epsilon_{cr2}$, plugging $\epsilon_{cr} = \epsilon_{cr1}$ and taking numerical parameters for Equation (C12), we obtain

$$J_C = 8.8 \times 10^{14} \left(\frac{\text{AU}}{R} \right)^2 a_{-5}^3 \gamma_4 \exp \left(-\frac{4.0 a_{-5}^{1/4} \hat{\rho}^{1/4}}{\gamma_4} \right) \text{ s}^{-1}, \quad (\text{C13})$$

where $\gamma_4 = \gamma/10^4$.¹¹

The grain charge at 1 AU is evaluated as the following:

$$Z_C(1 \text{ AU}) = \int dt J_C = \int_{R_i}^{1 \text{ AU}} \frac{dR}{\gamma c \beta} J_C. \quad (\text{C14})$$

Plugging (C13) into the above equation and carrying out the simple integration, we obtain

$$\begin{aligned} Z_C(1 \text{ AU}) &= 8.8 \times 10^{10} \left(\frac{\text{AU}}{c\beta} \right) a_{-5}^3 \exp \left(-\frac{0.4 a_{-5}^{1/4} \hat{\rho}^{1/4}}{\gamma_5} \right), \\ &= 4.4 \times 10^{13} a_{-5}^3 \beta^{-1} \exp \left(-\frac{0.4 a_{-5}^{1/4} \hat{\rho}^{1/4}}{\gamma_5} \right). \end{aligned} \quad (\text{C15})$$

D. VELOCITY, MOMENTUM AND ENERGY

Let E be the kinetic energy of the particle, γ be the Lorentz factor and $\beta = v/c$. In this paper, the particle energy is implicitly referred to as its kinetic energy. The momentum of the particle is $p = \gamma\beta mc$. Let recall that the total energy of a particle is

$$E_{\text{tot}}^2 = E_0^2 + p^2 c^2 = E_0^2 + \beta^2 \gamma^2 E_0^2 = E_0^2 (1 + \beta^2 \gamma^2), \quad (\text{D1})$$

$$= E_0^2 \gamma^2 \quad (\text{D2})$$

where $E_0 = mc^2$ is the particle energy at rest, and $\gamma^2 = 1/(1 - \beta^2)$ has been used.

The kinetic energy is defined as

$$E = E_{\text{tot}} - E_0 = E_0 (\gamma - 1) \quad (\text{D3})$$

Thus, we can have the following relationships:

$$\gamma = 1 + \frac{E}{E_0}, \quad \beta = \frac{\sqrt{E(E + 2E_0)}}{E + E_0}. \quad (\text{D4})$$

¹¹ A typo of $\gamma^{3/4}$ in Eq. (A28) of Bingham et al. (1999) fixed.

REFERENCES

- Accardo et al. 2014, PRL 113, 121101
- Aguilar et al. 2014, PRL 113, 121102
- Andersson B.-G., Lazarian A., Vaillancourt J., 2015, AR& AA
- Abbasi, R. U., Abu-Zayyad, T., Allen, M., & et al. 2008, *Astroparticle Physics*, 30, 175
- Abraham, J., Abreu, P., Aglietta, M., & et al. 2007, *Science*, 318, 938
- Abreu, P., Aglietta, M., Ahn, E. J., & et al. 2010, *Astroparticle Physics*, 34, 314
- Alfvén, H. 1954, *Tellus*, 6, 232
- Aloisio, R., Berezhinsky, V., & Gazizov, A. 2012, *Astroparticle Physics*, 39, 129
- Anchordoqui, L. A. 2000, *Physical Review D (Particles)*, 61, 87302
- Beresnyak, A., Jones, T. W., & Lazarian, A. 2009, *ApJ*, 707, 1541
- Berezhko, E. G., Ksenofontov, L. T., & Völk, H. J. 2003, *A&A*, 412, L11
- Berezinskii, V. S., & Prilutskii, O. F. 1977, In: *International Cosmic Ray Conference*, 2, 358
- Berezinsky, V., Gazizov, A., & Grigorieva, S. 2006, *Physical Review D*, 74, 43005
- Berezinsky, V. S., & Prilutsky, O. F. 1973, *Astrophysics and Space Science*, 21, 475
- Bethe, H., & Heitler, W. 1934, *Proceedings of the Royal Society A: Mathematical, Physical and Engineering Sciences*, 146, 83
- Bingham, R., Bingham, R., Tsyтовich, V. N., & Tsyтовich, V. N. 1999, *Astroparticle Physics*, 12, 35
- Blandford, R. D., Blandford, R. D., Ostriker, J. P., & Ostriker, J. P. 1978, *ApJ*, 221, L29
- Bringa, E. M., & Johnson, R. E. 2000, *Surface Science*, 451, 108
- Bringa, E. M., & Johnson, R. E. 2002, *Physical Review Letters*, 88, 165501
- Bringa, E. M., & Johnson, R. E. 2003, in *Solid state astrochemistry. Proceedings of the NATO Advanced Study Institute on Solid State Astrochemistry*, 357–393
- Bringa, E. M., & Johnson, R. E. 2004, *The Astrophysical Journal*, 603, 159
- Bringa, E. M., Johnson, R. E., & Dutkiewicz, . 1999a, *Nuclear Instruments and Methods in Physics Research Section B*, 152, 267
- Bringa, E. M., Johnson, R. E., & Jakas, M. 1999b, *Physical Review B (Condensed Matter and Materials Physics)*, 60, 1380475
- Bringa, E. M., Kucheyev, S. O., Loeffler, M. J., et al. 2007, *The Astrophysical Journal*, 662, 372
- Cho, J., & Lazarian, A. 2002, *Physical Review Letters*, 88, 245001
- Cho, J., & Lazarian, A. 2003, *MNRAS*, 345, 325
- Dasgupta, A. K. 1979, *Astrophysics and Space Science*, 63, 517
- de Gouveia Dal Pino, E. M., & Lazarian, A. 2005, *A&A*, 441, 845
- Dermer, C. D., & Schlickeiser, R. 2002, *ApJ*, 575, 667
- Draine, B. T. 2003, *ApJ*, 598, 1026
- Draine, B. T. 2011, *ApJ*, 732, 100
- Draine, B. T. 2011, *Physics of the Interstellar and Intergalactic Medium* (Princeton, NJ: Princeton Univ. Press)
- Draine, B. T., & Salpeter, E. E. 1979a, *ApJ*, 231, 438
- Draine, B. T., & Salpeter, E. E. 1979b, *ApJ*, 231, 77
- Draine, B. T., & Sutin, B. 1987, *ApJ*, 320, 803
- Dwek, E., & Smith, R. K. 1996, *Astrophysical Journal* v.459, 459, 686
- Elenskii, Y. S., & Suvorov, A. L. 1977, *Astrophysics*, 13, 432
- Ellison, D. C., Drury, L. O., & Meyer, J.-P. 1997, *ApJ*, 487, 197
- Epstein, R. I. 1980, *MNRAS*, 193, 723
- Eyink, G. L., Lazarian, A., & Vishniac, E. T. 2011, *ApJ*, 743, 51
- Fano, U. 1963, *Annual Review of Nuclear and Particle Sciences*, 13, 1
- Fleischer, R. L., Price, P. B., & Walker, R. M. 1965, *Journal of Applied Physics*, 36, 3645
- Giacalone, J., Giacalone, J., Jokipii, J. R., & Jokipii, J. R. 2009, *ApJ*, 701, 1865
- Greisen, K. 1966, *Physical Review Letters*, 16, 748
- Grindlay, J. E., & Fazio, G. G. 1974, *ApJ*, 187, L93
- Guahthakurta, P., & Draine, B. T. 1989, *ApJ*, 345, 230
- Hayakawa, S. 1972a, *Ap&SS*, 16, 238
- Hayakawa, S. 1972b, *Ap&SS*, 19, 173
- Herlofson, N. 1956, *Tellus*, 8, 268
- Hoang, T., & Lazarian, A. 2012, *ApJ*, 761, 96
- Hoang, T., Lazarian, A., & Schlickeiser, R. 2012, *ApJ*, 747, 54
- Inokuti, M. 1971, *Review of Modern Physics*, 43, 297
- Itoh, N., Duffy, D. M., Khakshouri, S., & Stoneham, A. M. 2009, *Journal of Physics: Condensed Matter*, 21, 4205
- Ivlev, A. V., Lazarian, A., Tsyтовich, V. N., et al. 2010, *ApJ*, 723, 612
- Johnson, R. E., & Brown, W. L. 1982, *Nuclear Instruments and Methods In Physics Research*, 198, 103
- Johnson, R. E., Pospieszalska, M., & Brown, W. L. 1991, *Physical Review B*, 44, 7263
- Johnson, R. E., & Schou, J. 1993, in *Fundamental Processes in the Sputtering of Atoms and Molecules*, ed. P. Sigmund (Royal Danish Academy, Copenhagen), 403
- Khan, S. A., Tripathi, A., Toulemonde, M., Trautmann, C., & Assmann, W. 2013, *Nuclear Inst. and Methods in Physics Research*, B, 314, 34
- Kowal, G., de Gouveia Dal Pino, E. M., & Lazarian, A. 2012, *Physical Review Letters*, 108, 241102
- Kowal, G., & Lazarian, A. 2010, *ApJ*, 720, 742
- Kowal, G., Lazarian, A., Vishniac, E. T., & Otmianowska-Mazur, K. 2009, *ApJ*, 700, 63
- Lazarian, A. 2005, in *AIP Conf. Ser.*, Vol. 784, *Magnetic Fields in the Universe: From Laboratory and Stars to Primordial Structures*, ed. E. M. de Gouveia dal Pino, G. Lugones, & Lazarian, A., 42–53
- Lazarian, A., & Desiati, P. 2010, *ApJ*, 722, 188
- Lazarian, A., & Opher, M. 2009, *ApJ*, 703, 8
- Lazarian, A., & Vishniac, E. T. 1999, *ApJ*, 517, 700
- Lazarian, A., & Yan, H. 2002, *ApJ*, 566, L105
- Lazarian, A., & Yan, H. 2014, *ApJ*, 784, 38
- Linsley, J. 1980, *Astrophysical Journal*, 235, L167
- Longair, M. S. 2011, *High Energy Astrophysics* (Cambridge: Cambridge University Press)
- Mathis, J. S., Mezger, P. G., & Panagia, N. 1983, *A&A*, 128, 212
- Mathis, J. S., Rumpl, W., & Nordsieck, K. H. 1977, *ApJ*, 217, 425
- Matsunami, N., Sataka, M., & Iwase, A. 2002, *Nuclear Instruments and Methods in Physics Research Section B*, 193, 830
- Matsunami, N., Sataka, M., Iwase, A., & Okayasu, S. 2003, *Nuclear Instruments and Methods in Physics Research B*, 209, 288
- Matsunami, N., Sataka, M., Okayasu, S., & Tazawa, M. 2007, *Nuclear Instruments and Methods in Physics Research Section B*, 256, 333
- McBreen, B., Plunkett, S., & Lambert, C. J. 1993, *Astrophysics and Space Science*, 205, 355
- Noerdlinger, P. D. 1971, *ApSS*, 13, 70
- Riquelme, M. A., & Spitkovsky, A. 2010, *ApJ*, 717, 1054
- Robertson, H. P. 1937, *MNRAS*, 97, 423
- Sanders, J. M., Dubois, R. D., Manson, S. T., et al. 2007, *Physical Review A*, 76, 62710
- Savvatimskiy, A. I. 2005, *Carbon*, 43, 1115
- Scoville, N., & Norman, C. 1995, *ApJ*, 451, 510
- Sigmund, P. 1981, *Sputtering by Particle Bombardment I*, 4, 9
- Sokolsky, P. 2013, *ISVHECRI 2012 - XVII International Symposium on Very High Energy Cosmic Ray Interactions*, 52, 06002
- Spitzer, L. 1949, *Physical Review*, 76, 583
- Sternheimer, R. M., Berger, M. J., & Seltzer, S. M. 1984, *Atomic Data and Nuclear Data Tables*, 30, 261
- Suga, K., Sakuyama, H., Kawaguchi, S., & Hara, T. 1971, *Physical Review Letters*, 27, 1604
- Tielens, A. G. G. M., McKee, C. F., Seab, C. G., & Hollenbach, D. J. 1994, *ApJ*, 431, 321
- Tombrello, T. A. 1994, *Nuclear Instruments and Methods in Physics Research Section B*, 94, 424
- Tsong, T. T., & Müller, E. W. 1970, *Physica Status Solidi (a)*, 1, 513
- Urbassek, H. M., Kafemann, H., & Johnson, R. E. 1994, *Physical Review B (Condensed Matter)*, 49, 786
- van de Hulst, H. C. 1957, *Light Scattering by Small Particles* (New York: John Wiley & Sons)
- Verner, D. A., Ferland, G. J., Korista, K. T., & Yakovlev, D. G. 1996, *ApJ*, 465, 487
- Waxman, E., & Draine, B. T. 2000, *ApJ*, 537, 796

Weingartner, J. C., & Draine, B. T. 2001, ApJS, 134, 263
Weingartner, J. C., Draine, B. T., & Barr, D. K. 2006, ApJ, 645,
1188

Wiscombe, W. J. 1980, Applied Optics, 19, 1505
Yan, H., Lazarian, A., & Draine, B. T. 2004, ApJ, 616, 895
Zatsepin, G. T., & Kuz'min, V. A. 1966, JETP, 4, 78